NISTIR 5755

Guide for X-Ray Powder Diffraction Analysis of Portland Cement and Clinker

Paul E. Stutzman

March, 1996
Building and Fire Research Laboratory
National Institute of Standards and Technology
Gaithersburg, MD 20899

U.S. Department of Commerce
Ronald H. Brown, *Secretary*
Technology Administration
Mary L. Good, *Under Secretary for Technology*

Abstract

Accurate, rapid methods for determining phase abundance are necessary to aid in classification of cements and for correlation of performance characteristics with composition. X-ray powder diffraction is a direct method for qualitative and quantitative phase abundance analysis of fine-grained materials. While the application of powder diffraction in the cement industry is well established for qualitative analysis, its use in the determination of phase abundance is not as common. This guide examines methods for compositional analysis of portland-cement clinker and cement by X-ray powder diffraction through examples of diffraction pattern profile regions used in phase and polymorph identification, and demonstration of a procedure for calibration and quantitative phase abundance analysis.

Keywords

clinker, phase composition, portland cement, quantitative analysis, qualitative analysis, X-ray powder diffraction

Table of Contents

	Page
Abstract	iii
1.0 Introduction	1
2.0 Experimental Procedure	2
2.1 Sample Preparation	3
2.1.1 Heat Treatment of Cements	3
2.2 Phase Identification	4
2.2.1 Alite	4
2.2.2 Belite	9
2.2.3 Aluminates	9
2.2.4 Ferrites	9
2.2.5 Alkali Sulfates	13
2.2.6 Calcium and Magnesium Oxides	13
2.2.7 Calcium Sulfates	16
2.3 Reference Compounds for Clinker Phases	16
3.0 Selective Extractions	
3.1 Potassium Hydroxide/Sugar Extraction (KOH/sugar)	18
3.2 Salicylic Acid/Methanol Extraction (SAM)	18
3.3 Nitric Acid/Methanol Extraction	21
4.0 Evaluating and Monitoring Machine Performance	21
5.0 Quantitative Analysis	24
5.1 The Internal Standard Method for Quantitative Analysis	24
5.2 The Reference Intensity Ratio Technique	26
6.0 Data Collection	27
6.1 Pattern Intensity Measurement	27
6.1.1 Peak Area Measurement	27
6.1.2 Whole-Pattern Fitting	28
6.2 Rietveld Method	28
7.0 ASTM C01.23.01 Cooperative Calibration	30
8.0 Summary and Conclusions	36
9.0 Acknowledgements	37
10.0 References	37

List of Tables

		Page
Table 1.	Common Phases in Clinker and Cement Analysis and Internal Standards	7
Table 2.	Mass Absorption Coefficients, μ/ρ, for Selected Phases Commonly Found in Clinker and Cement, and Internal Standards	24
Table 3.	Dataset for the Cooperative Calibration	33
Table 4.	X-Ray Powder Diffraction Intensity Data for Unknowns	35

List of Figures

Figure 1. Scheme for XRD characterization of clinker and cement..... 2

Figure 2. X-Ray powder diffraction patterns of NIST Reference clinkers 8486 (A), 8487 (B), and 8488 (C) with key peaks used for identification of alite, belite, aluminate, ferrite, and periclase. The greater peak intensities for periclase in RM 8486 and for aluminate in RM 8487 reflect their greater abundance..... 5

Figure 3. Powder diffraction patterns of (1), M1; 2, (M3), and 3, (T1) alite. The profile of the 51.5° peak is used to identify the alite polymorph. Mixtures of polymorphs are always possible..... 6

Figure 4. Powder diffraction patterns of (1), β-C_2S; (2), α-C_2S; (3), α'-C_2S; and (4), γ-C_2S illustrate the distinct differences in their diffraction patterns..... 10

Figure 5. Aluminate polymorphs are distinguished using the most intense peak around 33.3° followed by peaks around 20° to 23° 2θ. For illustration clarity, the relative intensities are not correct..... 11

Figure 6. Members of the calcium aluminoferrite solid solution series include (1), brownmillerite; (2), srebrodol'skite; and (3), and unnamed calcium aluminum iron oxide..... 12

Figure 7. Powder diffraction patterns of the common alkali sulfates..... 14

Figure 8. Powder diffraction patterns of free lime (CaO) and periclase (MgO)..... 15

Figure 9. X-ray powder diffraction patterns of the calcium sulfates..... 17

Figure 10. The potassium hydroxide / sugar extraction dissolves the interstitial phases aluminate and ferrite leaving a residue of silicates and periclase..... 19

Figure 11. The salicylic acid / methanol extraction dissolves the silicate phases leaving alite and belite, and free lime from the bulk clinker (lower pattern) leaving a residue enriched in ferrite, aluminate, and alkali sulfates 20

Figure 12. A residue enriched in ferrite and periclase may be obtained using a nitric acid/methanol extraction..... 22

Figure 13. Control charts for instrument sensitivity using SRM 1976 are used to determine machine accuracy in measurement of relative intensities. The lines indicate the upper and lower control limit boundaries as provided in the certificate..... 23

Figure 14. Background is fitted as a smooth curve to points selected as representative of the actual background. Peaks are resolved and background-subtracted peak areas calculated 29

Figure 15. Powder diffraction scans of cubic (A) and orthorhombic (B) aluminates, and a mixture containing both polymorphs (C). As the I 21.0° /I 21.8° ratio exceeds that of pure cubic aluminate (about 0.5), orthorhombic aluminate may be considered to be present (D)..... 32

Figure 16. Calibration curves and RIR values for ASTM round robin calibration..... 34

1.0 Introduction

Performance characteristics of cements are influenced by their phase composition. ASTM classification of cements as Types I through V are based partly on composition, with cements optimized for different applications. For example, the rapid strength development of Type III cements with their relatively larger mass fraction of alite. In contrast, the decreased mass fraction of alite and aluminate produces a lower heat Type IV cement. The development of low aluminate, sulfate-resistant Type V cement reflects the knowledge of the relationship between the aluminate phase and performance of cements in sulfate environments. The phenomena of flash and false set have been related to the amount and form of calcium sulfate in the cement [1]. The ability to accurately determine cement composition should lead to a better understanding of its effects on performance and aid in the prediction of concrete material properties.

Methods employed in phase composition analysis include microscopy, chemical analysis, and X-ray powder diffraction. Microscopical methods provide direct analysis suitable for clinker, but due to the small particle size, are rarely applied to ground cements. The small crystal size of some phases often make their identification and quantitative determination by microscopy a difficult, time-consuming task. Chemical data are also used to determine the potential phase composition via the Bogue calculation. This is an indirect method, and the potential compositions are often in error as the compositions of the clinker phases are not those assumed in the calculation [1].

X-ray powder diffraction (XRD) is a direct method for qualitative and quantitative characterization of fine-grained materials such as clinker and cement, and may also be used for analysis of raw materials. Each phase produces a unique diffraction pattern independent of others, with the intensity of each pattern proportional to that phases concentration in a mixture.

This guide addresses procedures for XRD analysis of portland-cement clinker and cement and includes information on reference standards, sample preparation, selective extraction techniques, and both qualitative and quantitative analysis. These procedures will be illustrated using a data set produced for the ASTM C01.23.01 task group cooperative calibration [2,3].

2.0 Experimental Procedure

Figure 1 outlines a typical set of procedures involved in qualitative and quantitative XRD analysis of a clinker or cement. Selective extractions are not a necessary portion of an analysis, they serve to concentrate certain phase groups thereby facilitating their study.

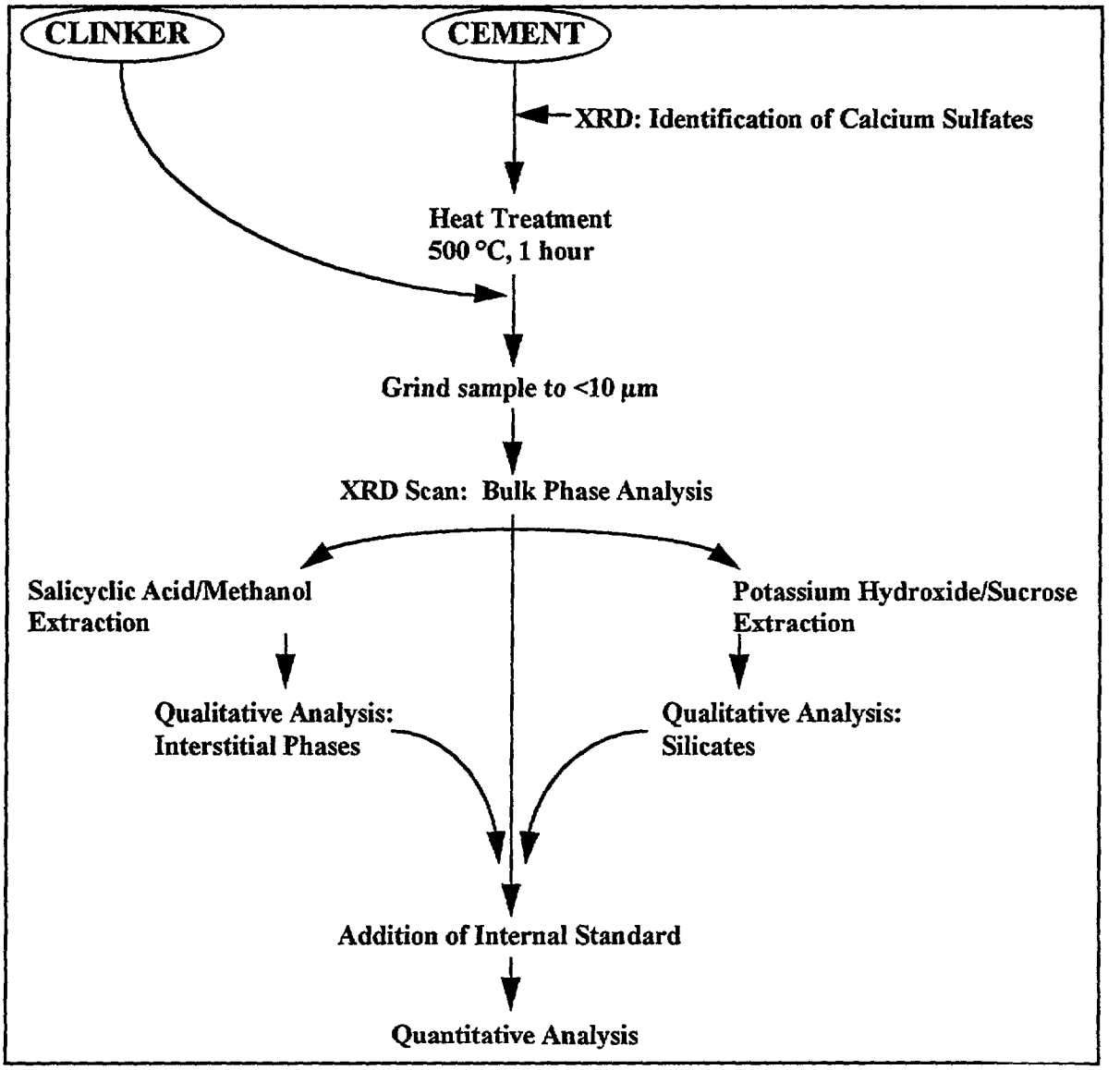

Figure 1. Scheme for XRD characterization of clinker and cement

2.1 Sample Preparation

Careful, consistent sample preparation is necessary to obtain a representative, homogeneous sample for analysis. Critical factors identified by Klug and Alexander [4] include particle and crystallite size, sample thickness, preferred orientation, strain, and surface planarity.

Grinding to reduce particle size to between 1 and 10 μm helps in minimizing a number of potential problems. A small particle size produces strong intensity diffraction patterns while lessening the influence of problems such as microabsorption, extinction, preferred orientation, and sample homogeneity, all of which can result in peak intensity errors [4]. A variety of grinding mills are capable of producing suitable particle size distributions, provided the material is wet-ground [5]. Over grinding or dry grinding may strain the crystallites or produce an appreciable amorphous surface layer, indicated by a decrease in peak intensity and an increase in peak width [4]. The procedure found suitable involves a ten-minute wet grind in 200-proof ethanol using a Micronizing Mill,[1,2] followed by vacuum filtering the powder on a 0.45μm filter and Buchner funnel, and drying at 60 °C. As cements are moisture sensitive, storage in a vacuum desiccator is recommended and should eliminate hydration problems.

2.1.1 Heat Treatment of Cements

Gypsum is added to control setting of portland cements, though possible impurities in its source or processing that may induce phase changes, and other calcium sulfate-water forms may be present. Identification of calcium sulfates in cements is made from a diffraction scan of the cement as received; that is, prior to laboratory grinding or other treatment. Then heating the cement sample at 500 °C for one hour drives off the water, converting each form to anhydrite. This simplifies analysis through measurement of only one calcium sulfate phase, eliminates peak overlaps since gypsum peaks interfere with aluminates and belite, and provides a single resolvable, intense diffraction peak for measurement.

---

[1]McCrone Micronizing Mill, McCrone Research, Westmont, IL

[2]Mention of brand names is made to provide complete details of the experimental procedure. In no case does such identification imply recommendation or endorsement by the National Institute of Standards and Technology, nor does it imply that the products are the best available for the purpose.

2.2 Phase Identification

Cement clinker is comprised of four major phases: alite (C_3S[3], 50-70%, by mass), belite (C_2S, 15-30%), aluminate (C_3A, 0-15%), ferrite (C_4AF, 5-15%); and minor phases: periclase (M), calcium oxide (C), and alkali sulfates ($(K\text{-}Na_2)SO_4$) [1]. Cement contains additions of gypsum and possibly other calcium sulfates (2-6%). Clinker and cement phase powder diffraction patterns are complex and the number of phases creates a composite pattern with many peak overlaps. With most of the strong diffraction peaks overlapping, identifications and measurements are often made using the weaker peaks. Figure 2 illustrates diffraction patterns of the three NIST Reference Material clinkers, labeling peaks that are key in recognition of the silicate and interstitial phases. Comparison of peak intensities also provides some indication of the relative phase abundances.

Table 1 is an updated list of clinker and cement compounds from Highway Research Board Special Report 127 [6] on phases in cement and concrete, presenting the eight strongest diffraction peak 2θ values and relative intensities. All references to diffraction peak 2θ values assume the use of copper $K\alpha$ radiation. The reference card numbers and relative intensities for the eight strongest peaks (rounded to the nearest 10%) have been obtained from the International Center for Diffraction Data (ICDD, formerly JCPDS) database [7]. Identifications should be confirmed through comparison with the complete diffraction pattern provided on the ICDD card.

2.2.1 Alite

The term alite is used in reference to impure forms of C_3S which may incorporate Mg^{2+}, Al^{3+}, and Fe^{3+}. Alite forms the bulk of the clinker and is important for strength development at early ages (<28 days) [1]. Three polymorphs of alite thought to commonly occur in industrial clinkers are distinguished by the profile of the diffraction lines occurring around 51° to 51.5° 2θ. As illustrated in Figure 3, the M1 polymorph is distinguished by a single peak at 51.7° 2θ (although the ICDD card exhibits a doublet); M3 by a well-defined doublet at 51.7° 2θ; and the triclinic T1 polymorph exhibits a triplet between 51° and 52° 2θ [1]. Strong, resolvable peaks for intensity measurements for quantitative analysis include one at 30.4° and another at 51.7° 2θ.

---

[3] Cement chemists have developed an abbreviated notation for specification of each compound where the oxides comprising that phase are represented by a single letter. The following abbreviations are used: SiO_2 (S); Al_2O_3 (A); Fe_2O_3 (F); CaO (C); MgO (M); SO_3 ($\bar{S}$); Na_2O (N); and K_2O (K).

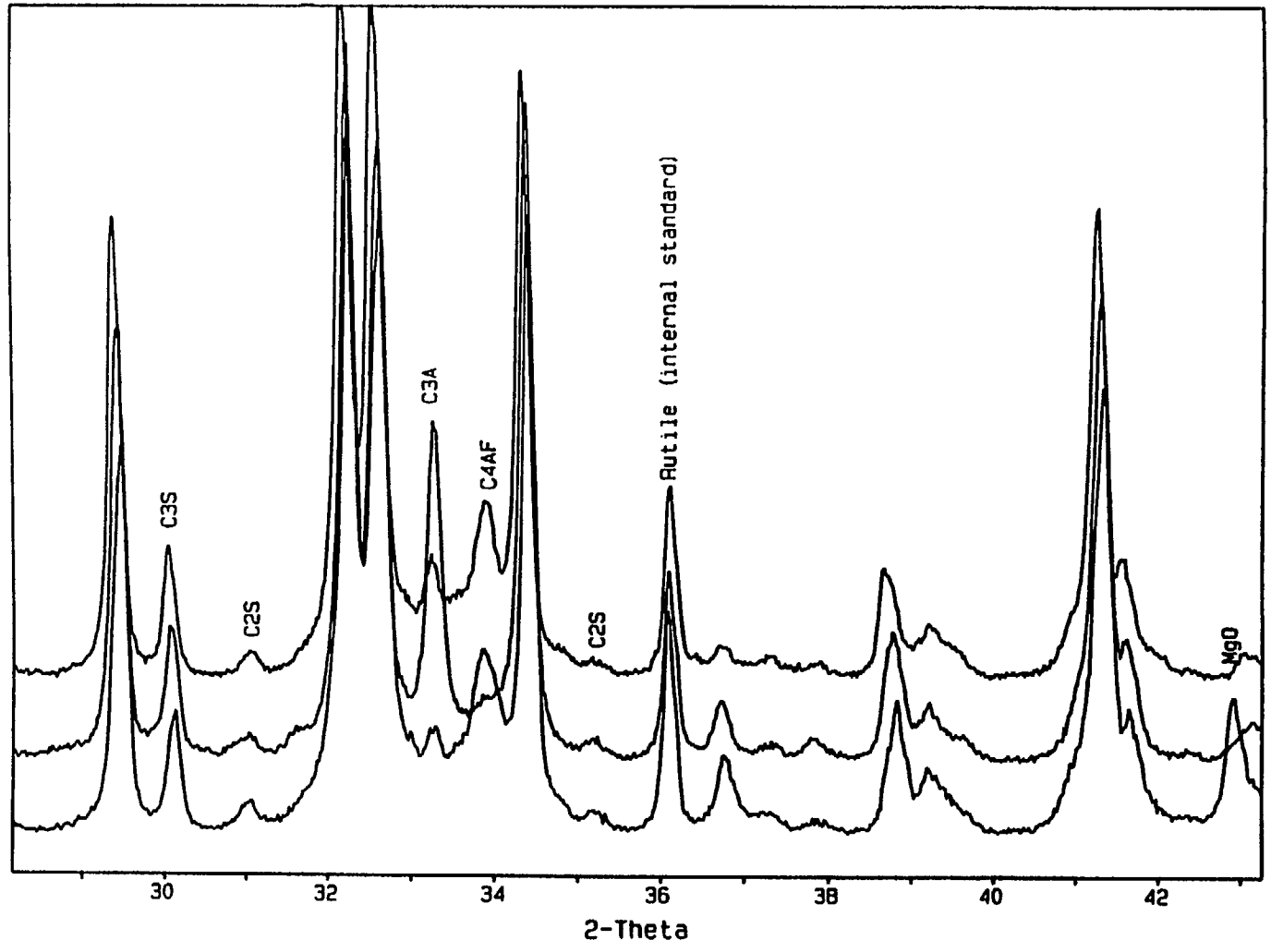

Figure 2. X-ray powder diffraction patterns of NIST Reference Clinkers 8486 (A), 8487 (B), and 8488 (C) with key peaks used for identification of alite, belite, aluminate, ferrite, and periclase. The greater peak intensities for periclase in RM 8486 and for aluminate in RM 8487 reflect their greater abundance.

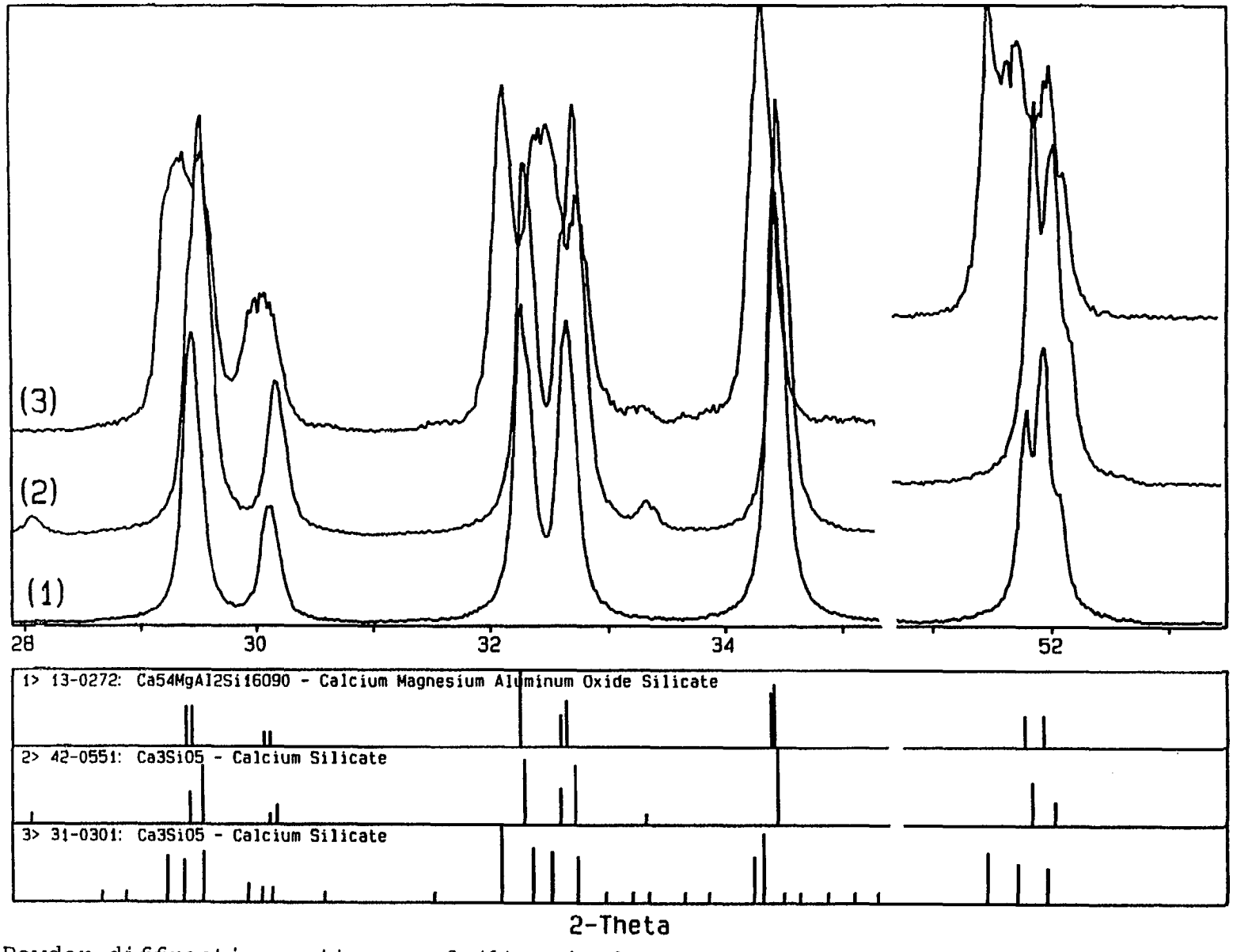

Figure 3. Powder diffraction patterns of (1), M1; 2, (M3), and 3, (T1) alite. The profile of the 51.5° peak is used to identify the alite polymorph. Mixtures of polymorphs are always possible.

Table 1. Common Phases in Clinker and Cement Analysis and Internal Standards [111].

Compound	Name	ICDD Database Principal Diffraction Peaks (Degrees 2θ)
Oxides and Hydrated Oxides		
calcium oxide	lime	37-1497 37.35_x, 53.86_5, 32.20_4, 64.15_2, 67.38_2, 91.46_2, 147.78_2, 0.98_1
magnesium oxide	periclase	4-829 42.91_x, 62.31_5, 78.61_1, 109.73_2, 127.19_2, 36.95_1, 93.99_1, 74.68_1
silicon dioxide	quartz	33-1161 26.65_x, 20.85_2, 50.14_1, 59.95_1, 36.54_1, 39.46_1, 68.13_1, 67.75_1
calcium hydroxide	portlandite	4-733 34.09_x, 18.09_7, 47.12_4, 50.79_4, 28.66_2, 54.34_2, 62.54_1, 64.23_1
magnesium hydroxide	brucite	7-239 38.02_x, 18.59_9, 50.86_6, 58.64_4, 62.08_2, 68.26_2, 72.03_1, 81.26_1
Carbonates		
calcium carbonate	calcite	5-586 29.41_x, 39.40_2, 43.15_2, 47.49_2, 48.51_2, 35.97_1, 23.02_1, 57.40_1
calcium carbonate	aragonite	41-1475 26.21_x, 33.13_6, 45.85_6, 27.22_5, 37.88_5, 36.18_4, 38.41_3, 38.61_3
calcium carbonate	vaterite	33-268 27.05_x, 32.78_9, 50.08_7, 24.90_7, 43.85_6, 49.10_3, 55.81_3, 21.01_3
calcium magnesium carbonate	dolomite	36-426 30.94_x, 41.43_2, 44.95_1, 50.53_1, 51.07_1, 37.38_1,
magnesium carbonate	magnesite	8-479 32.63_x, 42.99_5, 53.89_4, 35.85_2, 46.82_1, 69.35_1, 70.30_1, 114.99_1
Sulfates		
calcium sulfate	anhydrite	37-1496 25.44_x, 31.37_3, 38.64_2, 40.82_2, 48.68_2, 55.72_2, 52.23_1, 41.31_1
calcium sulfate	soluble anhydrite	37-184 25.44_x, 31.32_8, 38.58_5, 40.78_5, 48.60_5, 55.66_5, 45.38_3, 49.06_3
calcium sulfate hemihydrate	bassanite	41-224 29.69_x, 31.90_4, 14.72_8, 25.67_5, 49.36_3, 49.24_2, 54.14_2, 55.10_2
calcium sulfate dihydrate	gypsum	33-311 11.59_x, 20.72_x, 29.11_8, 31.10_5, 33.34_4, 43.34_3, 23.40_2, 47.84_2
Alkali sulfates		
sodium,potassium sulfate	aphthitalite	20-926 32.20_x, 31.46_8, 22.39_7, 45.67_5, 25.27_2, 56.98_2, 57.44_2, 38.29_1
potassium sulfate	arcanite	5-613 30.78_x, 29.75_8, 30.96_5, 21.26_3, 37.09_3, 43.28_3, 43.43_3, 21.34_2
potassium calcium sulfate	calcium langbeinite	20-867 27.64_x, 26.87_x, 27.23_8, 32.22_5, 32.10_5, 32.53_5, 20.86_3, 21.03_3
sodium sulfate	thenardite	37-1465 32.12_x, 19.04_7, 28.99_6, 28.03_5, 33.83_5, 48.78_4, 38.62_3, 23.15_2
sodium sulfate, form I	metathenardite	1-990 31.70_x, 33.67_x, 22.96_6, 24.99_4, 47.05_4, 19.28_1, 58.77_1, 62.73_1
α-sodium sulfate		27-791 22.55_x, 31.19_9, 33.12_9, 24.64_3, 46.13_3, 18.83_2, 38.34_2, 40.49_2
sodium sulfate form III		24-1132 31.83_x, 33.98_5, 22.61_4, 23.59_3, 25.54_3, 37.82_2, 46.21_2, 52.49_2
potassium calcium sulfate hydrate	syngenite	28-739 31.31_x, 28.17_8, 15.51_6, 32.64_6, 31.62_5, 9.31_4, 19.18_4, 26.61_4
α-potassium sulfate		25-681 30.28_x, 28.13_x, 20.54_6, 41.81_5, 21.98_3, 36.88_1, 55.08_1, 17.34_1
sodium sulfate-10-hydrate	mirabilite	11-647 16.13_x, 27.77_8, 27.34_6, 28.68_6, 18.59_5, 23.21_4, 35.66_4, 31.93_3
calcium silicate sulfate hydroxide	hydroxyl ellestadite	25-173 31.49_x, 32.67_6, 31.93_5, 33.73_5, 49.13_5, 25.73_4, 62.54_2, 46.28_2

Tricalcium Silicates, alite

M1		13-272	32.22_{X}, 34.36_{8}, 32.61_{6}, 29.37_{5}, 29.42_{5}, 32.56_{4}, 41.31_{4}, 51.72_{4}
M3		42-551	34.41_{X}, 32.26_{9}, 29.51_{9}, 32.56_{9}, 41.37_{9}, 51.78_{9}, 32.56_{8}, 29.40_{8}
T1		31-301	32.07_{X}, 34.29_{9}, 41.15_{8}, 32.33_{7}, 29.52_{7}, 32.49_{7}, 51.41_{7}, 29.20_{6}

Dicalcium Silicates, belite

β-dicalcium silicate	larnite	33-302	32.14_{X}, 32.05_{X}, 32.59_{8}, 41.21_{5}, 34.33_{4}, 32.93_{3}, 45.74_{2}, 31.77_{2}
α-dicalcium silicate		23-1042	33.03_{X}, 31.80_{8}, 46.54_{6}, 40.53_{4}, 58.20_{4}, 22.78_{2}, 59.10_{2}
α'-dicalcium silicate	bredigite	20-237	32.57_{X}, 33.28_{8}, 41.27_{5}, 19.07_{3}, 23.33_{3}, 26.43_{3}, 31.10_{3}, 38.00_{3}
γ-dicalcium silicate		31-297	32.79_{X}, 29.64_{8}, 32.53_{7}, 47.61_{6}, 23.28_{5}, 20.56_{5}, 54.26_{4}, 50.58_{3}

Calcium Aluminates

calcium aluminate - cubic		38-1429	33.17_{X}, 47.63_{3}, 59.27_{2}, 21.76_{1}, 40.93_{1}, 69.64_{1}, 32.09_{1}, 79.34_{1}
sodium calcium aluminate - orthorhombic		32-150	33.24_{X}, 59.03_{X}, 40.88_{8}, 47.33_{8}, 48.08_{8}, 69.77_{6}
sodium calcium aluminate - tetragonal		26-957	33.24_{x}, 32.98_{6}, 47.33_{4}, 59.05_{4}, 48.13_{2}, 59.56_{2}, 69.82_{1}

Calcium Ferrites and Aluminoferrites

Calcium aluminoferrite solid solution series			
calcium aluminum ferrite	brownmillerite	30-226	33.88_{X}, 12.20_{5}, 50.23_{5}, 33.50_{4}, 44.12_{4}, 47.09_{4}, 32.13_{3}, 34.80_{2}
calcium ferrite	srebrodol'skite	38-408	11.99_{X}, 24.10_{X}, 33.46_{X}, 49.38_{X}, 46.64_{7}, 31.97_{6}, 33.03_{6}, 43.45_{4}
calcium aluminum ferrite		42-1469	34.07_{X}, 33.75_{5}, 47.52_{4}, 32.45_{3}, 44.34_{3}, 12.20_{2}, 24.48_{2}, 42.18_{2}

Internal Standards for Quantitative Analysis

titanium oxide	rutile	21-1276	27.45_{x}, 54.32_{6}, 36.09_{5}, 41.23_{3}, 56.64_{2}, 64.01_{2}, 69.79_{1}, 140.05_{1}
aluminum oxide	corundum	42-1468	43.36_{x}, 35.15_{x}, 57.50_{8}, 25.58_{7}, 68.21_{5}, 37.79_{4}, 52.56_{4}, 66.52_{3}
silicon	silicon	27-1402	28.44_{x}, 47.30_{6}, 56.12_{3}, 88.03_{1}, 76.38_{1}, 127.55_{1}, 114.09_{1}, 69.13_{1}
calcium fluoride	fluorite	35-816	47.01_{x}, 28.27_{9}, 55.77_{3}, 87.37_{2}, 68.67_{1}, 75.85_{1}, 126.20_{1}, 94.22_{1}

2.2.2 Belite

Impure dicalcium silicate, C_2S, is known as belite. The beta form predominates in industrial clinkers, although there are reports of α and α' forms. The presence of the poorly-reactive γ-C_2S is uncommon in industrial clinkers but, its presence is associated with dusting; cracking that may result in disintegration of the clinker [1]. While belite is less reactive than alite, it does contribute to later-age strengths. Identification of β-C_2S and intensity measurements for quantitative analysis are made using a resolvable peak at 31.0°, and a much weaker peak at 35.2° (Fig. 4) may also be used. The diffraction pattern of belite is difficult to observe and measure because the intense peaks are almost completely overlapped by those of alite.

2.2.3 Aluminates

Tricalcium aluminate, C_3A, incorporates impurities such as Si^{4+}, Fe^{3+}, Na^+, and K^+, and is the most reactive of the clinker phases. The presence of aluminate is indicated by its strongest peak around 33.3° (Fig. 5). Two polymorphs commonly encountered in industrial clinker, cubic and orthorhombic, are distinguished by examining the profiles and relative intensities of a set of diffraction peaks. A pseudo-tetragonal form is thought to be a modification of the orthorhombic form and exhibits a similar powder diffraction pattern [1]. The cubic variety exhibits strong singlet peaks at 33.3°, 47.7°, 59.4°, while the orthorhombic form exhibits splitting of the strong peak at 33.3° into a strong singlet at 33.2° and weaker close doublet at 32.9-33.0° [1]. The peaks in the 20° to 23° region may also be used to identify and quantify the aluminate polymorphs. These features may be more easily recognized in an extraction residue enriched in aluminate. Extraction procedures will be described in Section 3.0.

2.2.4 Ferrite

The ferrite phase occurs intermixed with tricalcium aluminate as an interstitial phase and forms a solid solution series with a composition range $Ca_2(Al_xFe_{1-x})_2O_5$, where x ranges from 0 to 0.7 [1]. C_4AF, representing a 1:1 Al:Fe ratio; $Ca_2(Al,Fe)_2O_5$, is known as brownmillerite. Other phases in the calcium aluminoferrite solid solution series include srebrodol'skite; $Ca_2Fe_2O_5$, and an unnamed calcium aluminum iron oxide; $Ca_2Al_{1.38}Fe_{0.62}O_5$. Key diffraction peaks in recognizing ferrite include those at 33.9° and 12.1°. While difficulties in resolving the 33.9° peak preclude its use in quantitative analysis, suitable peaks for intensity measurement include the 24.4° and 12.1° 2θ.

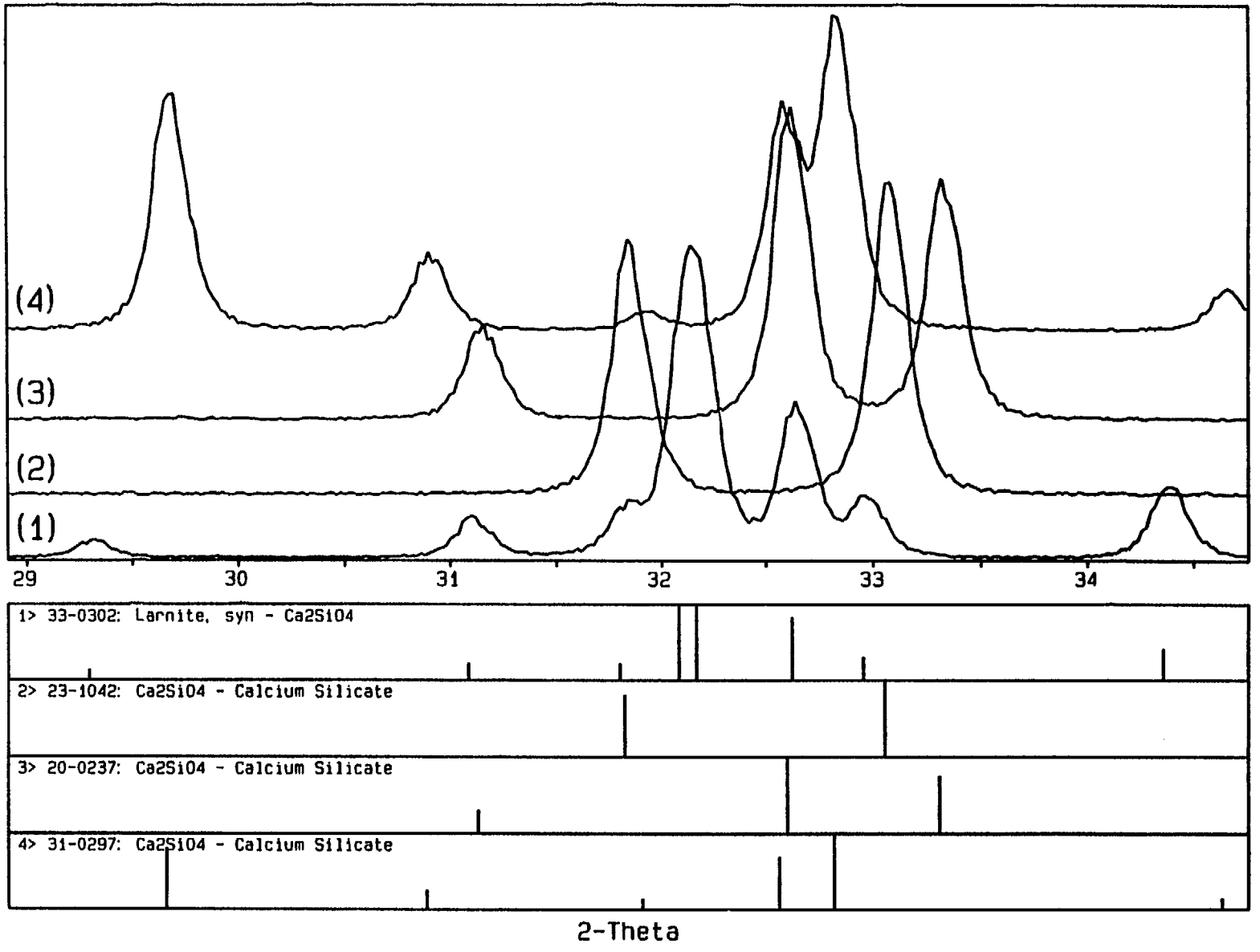

Figure 4. Powder diffraction patterns of (1), β-C_2S; (2), α-C_2S; (3), α'-C_2S; and (4) γ-C_2S illustrate the distinct differences in their diffraction patterns.

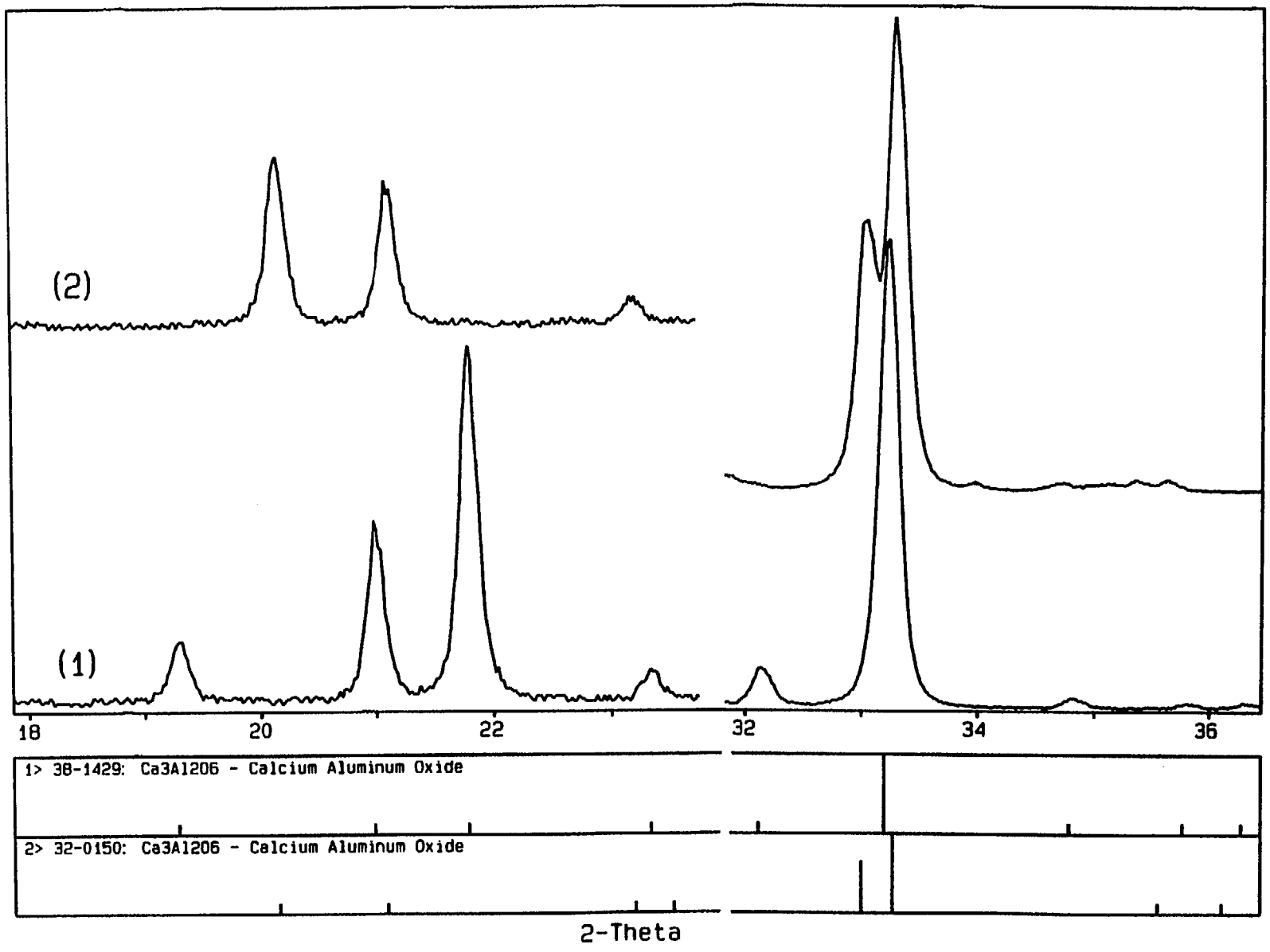

Figure 5. Aluminate polymorphs are distinguished using the most intense peak around 33.3° followed by peaks around 20° to 23° 2θ. For illustration clarity, the relative intensities are not correct.

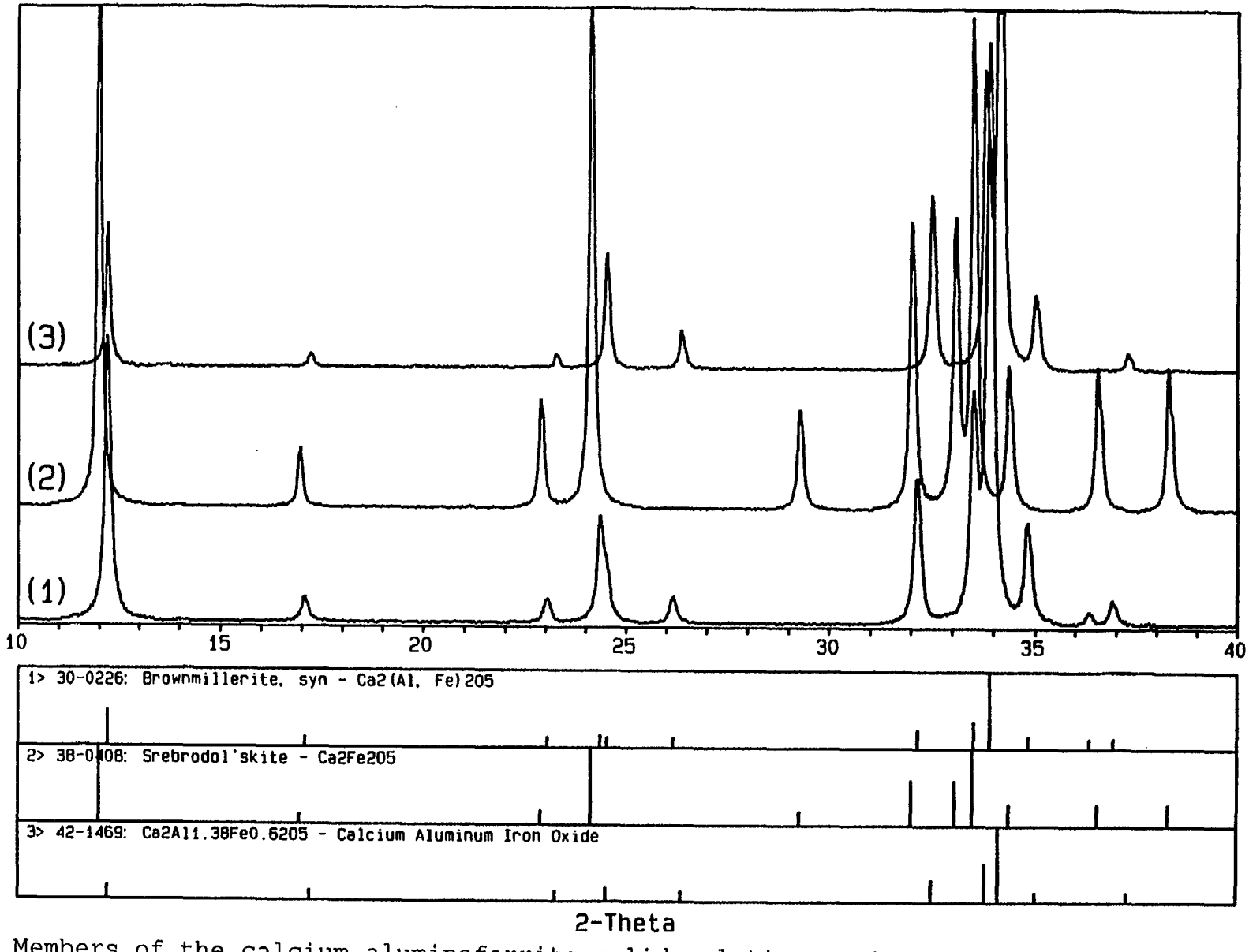

Figure 6. Members of the calcium aluminoferrite solid solution series include (1), brownmillerite; (2), srebrodol'skite; and (3), an unnamed calcium aluminum iron oxide.

2.2.5 Alkali Sulfates

Alkali sulfates are potassium or sodium sulfate compounds that are minor components in terms of mass fraction of a clinker or cement, but compounds that have been shown to influence concrete properties such as early- and late-age strength development and rheology [1]. Their low concentration in most clinkers and cements makes their identification difficult.

Three common alkali sulfates are aphthitalite, arcanite, and calcium langbeinite [8] (Fig. 7). The primary peaks of aphthitalite at 32.2° and 31.5° are overlapped by ferrite and the aluminates. The following peaks may be useful if the potential peak overlaps from other phases are considered: 1) 22.39° (I=70%) peak, with overlaps from minor ferrite (23°) and cubic aluminate (21.77°) peaks; 2) 25.3° peak (I=20%) overlapping a minor (I=1%) peak of cubic aluminate; and 3) the non-overlapped 18.4° peak (I=10%). Arcanite peaks at 29.77° (I=80%) and 21.3° (I=30) may be used, though the latter is located between the aluminate peaks at 20.9/21.0° and cubic aluminate at 21.7°. Calcium langbeinite produces a triple peak grouping around 27.3°, which is suitable for measurement. Identification is aided through concentration by using a salicylic acid/methanol extraction (section 3.0).

2.2.6 Calcium and Magnesium Oxides

Free lime (CaO) and periclase (MgO) (Fig. 8) are important because their presence creates a potential for expansion of mature concrete and subsequent durability problems. Free lime diffraction peaks at 37.3° and 53.9° may be used for identification and intensity measurement. The periclase diffraction peak at 42.8° may be used for identification and quantitative measurements. Free lime is very sensitive to its storage environment, readily reacting with moisture to form calcium hydroxide which may then carbonate to form calcite. The presence of calcium hydroxide, identified through its most intense diffraction peak at 18.1°, is an indication of exposure to moisture.

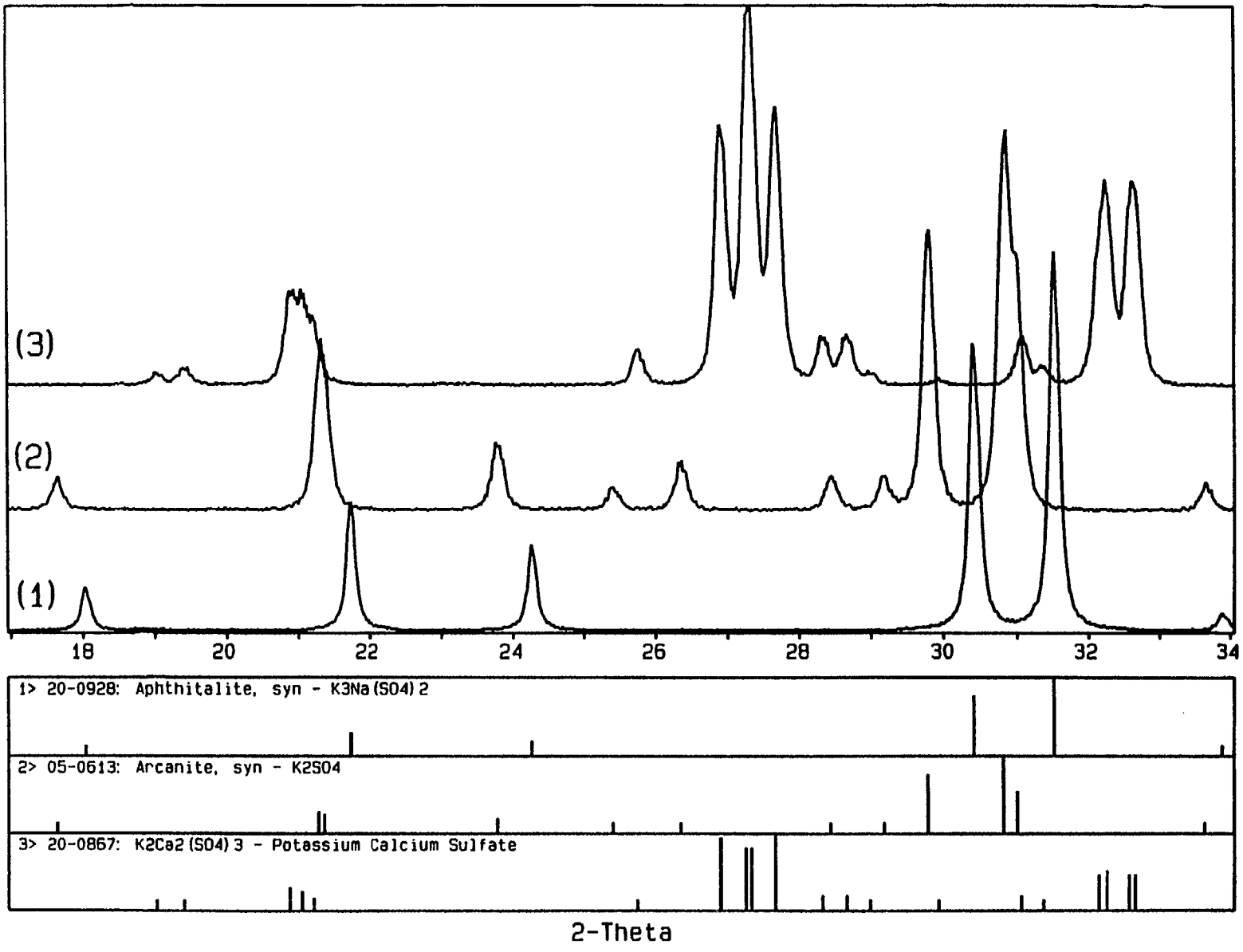

Figure 7. Powder diffraction patterns of the common alkali sulfates.

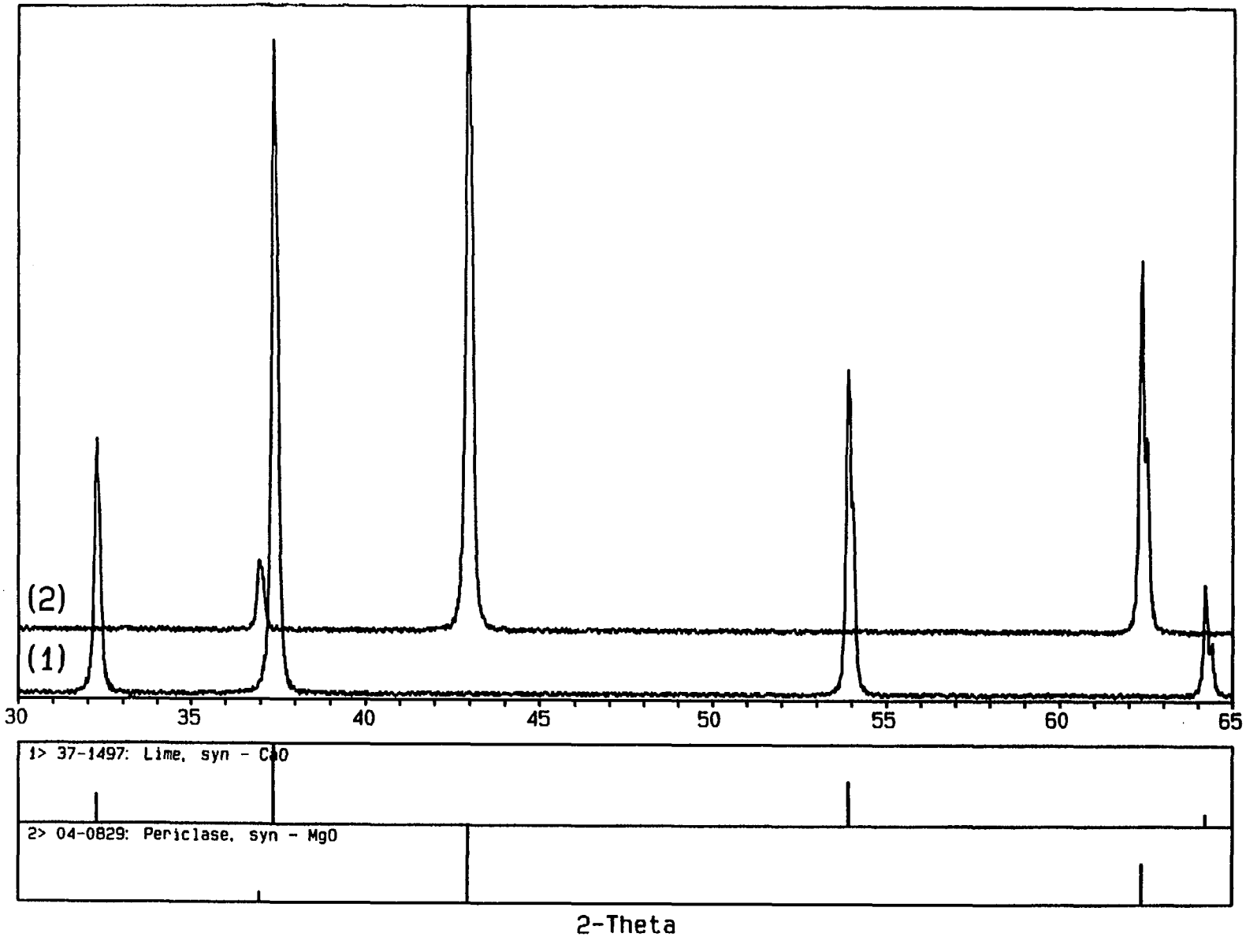

Figure 8. Powder diffraction patterns of free lime (CaO) and periclase (MgO).

2.2.7 Calcium sulfates

A number of calcium sulfate-water forms may be present in cement depending upon the composition of the gypsum added to clinker and the temperature and relative humidity encountered subsequent to the grinding process [1]. The primary forms include $CaSO_4 \cdot 2H_2O$ (gypsum), $CaSO_4 \cdot 1/2H_2O$ (bassanite, also known as hemihydrate), and $CaSO_4$ (anhydrite) (Fig. 9). Dehydration temperatures of about 70 °C and 100 °C, respectively, mark the approximate transitions between these phases. Another calcium sulfate form often called soluble anhydrite (γ-$CaSO_4$) is a dehydrated bassanite [9]. Identification of the calcium sulfate form is of interest as the relative solubilities (bassanite > soluble anhydrite > gypsum > anhydrite) affects the supply of SO_4^{2-} ions in the concrete [1]. Low angle peaks are used to identify gypsum (11.5° and 20.7°), bassanite (14.74°), and soluble anhydrite or anhydrite (25.48°). Though exhibiting a similar diffraction pattern, soluble anhydrite is distinguished from anhydrite by its stronger relative peak intensities.

2.3 Reference Compounds for Clinker Phases

Pure clinker phase standards may be purchased from commercial suppliers[4], synthesized in the laboratory, or for some phases, separated from the clinker by selective extraction methods. The ICDD database [7] often provides a description of procedures for synthesis of the phases.

[4]Pure cement compounds, triclinic and monoclinic C_3S, β-C_2S, cubic and orthorhombic C_3A, and C_4AF may be purchased from Construction Technology Laboratories, Skokie, IL, (800)-522-2CTL.

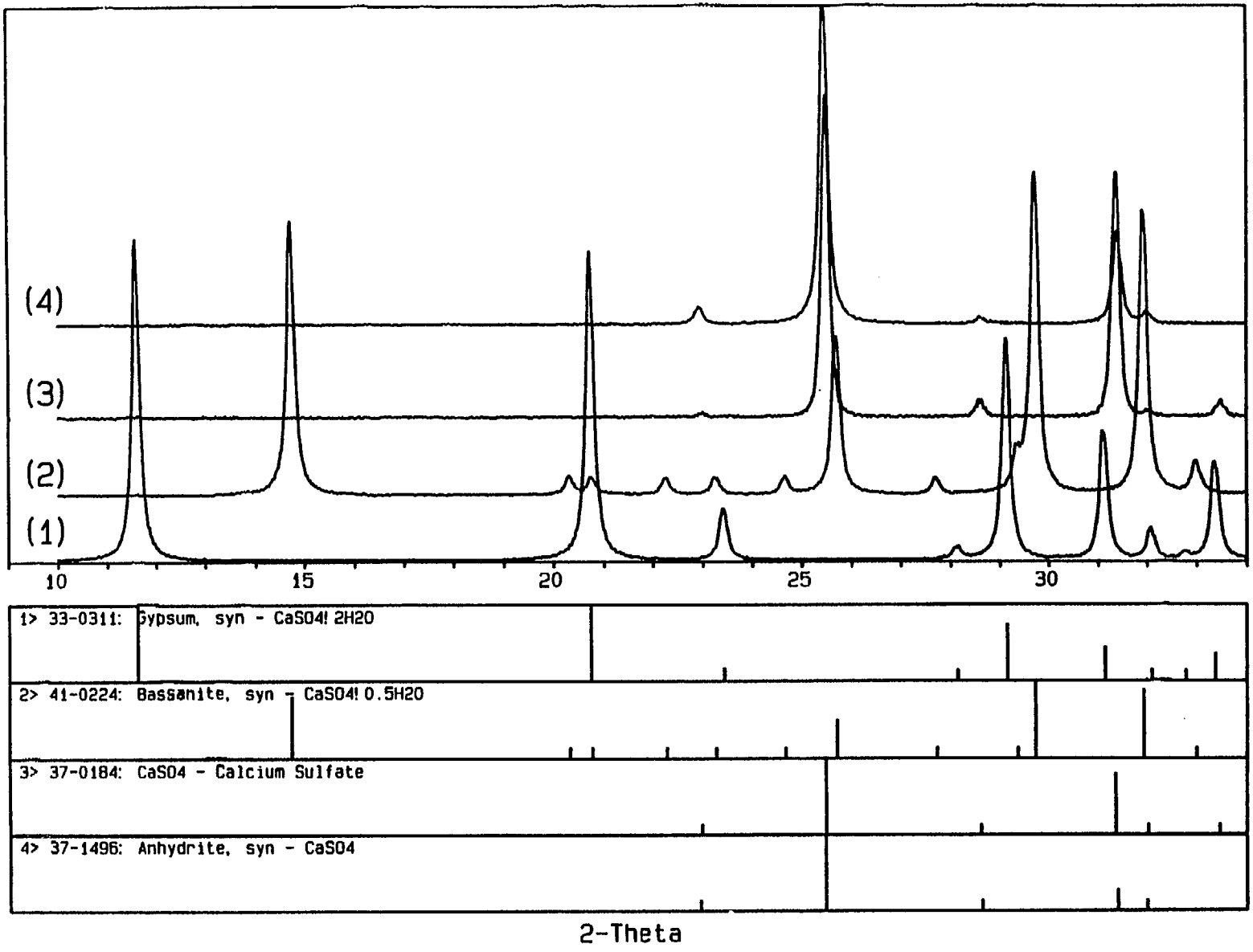

Figure 9. X-ray powder diffraction patterns of the calcium sulfates.

3.0 Selective Extractions

With cement compositions typically including six or more phases, diffraction patterns are often complicated because of partial or complete peak overlaps. Details of peak profiles necessary for polymorph identification may become ambiguous. Also, the lower intensity diffraction patterns of the less abundant interstitial and minor phases are often difficult to identify and quantify. Selective extraction techniques facilitate improved detection limits for identification and quantitative measurements by minimizing or eliminating the effects of dilution and overlap by selectively removing certain phases (Fig. 10). Quantitative extractions may also provide an additional estimate of phase fractions. The procedures detailed here were taken from Taylor [1], Gutteridge [10], and Klemm et. al [11].

3.1 Potassium Hydroxide/Sugar Extraction (KOH/sugar)

The KOH/sugar extraction dissolves the interstitial phases of aluminate and ferrite leaving a residue of silicates and minor phases such as periclase (Fig. 10). First, prepare an extraction solution of 30 g of KOH and 30 g of sucrose in 300 ml of water. Then stir about 9 g of powdered cement in a 95 °C KOH/sugar solution for one minute. Filter the solution using a 0.45µm filter and Buchner funnel, wash residue with 50 ml of water followed by 100 ml of methanol, dry the residue at 60 °C, and store in a vacuum desiccator.

Vacuum filtering fine clinker or cement powder extraction suspensions can often be difficult. To minimize problems, do not exceed the recommended extraction times and permit the suspension to settle prior to filtering or to centrifuging the suspension. Alternatively, extract and filter a coarser particle size sample. Because of the much larger particle size, care must be taken to ensure that the extraction has removed all the intended phases.

3.2 Salicylic Acid/Methanol Extraction (SAM)

The SAM extraction is used to dissolve alite, belite, and free lime leaving a residue of interstitial phases aluminate and ferrite as well as minor phases periclase and alkali sulfates (Fig. 11). Stir about 5 g of powdered cement in a stoppered flask containing 300 ml of SAM solution, consisting of 20 g salicylic acid in 300 ml of methanol, for two hours. Allow the suspension to settle for about 15 minutes then vacuum filter using a 0.45 µm filter and Buchner funnel. Wash the residue with methanol, dry at 90 °C, and store in a vacuum desiccator.

Gutteridge [12] used a modified SAM method combined with the KOH/sugar extraction to obtain residues enriched in belite. In this procedure, the mass of salicylic acid was adjusted to five times the mass of alite as estimated by the Bogue calculation.

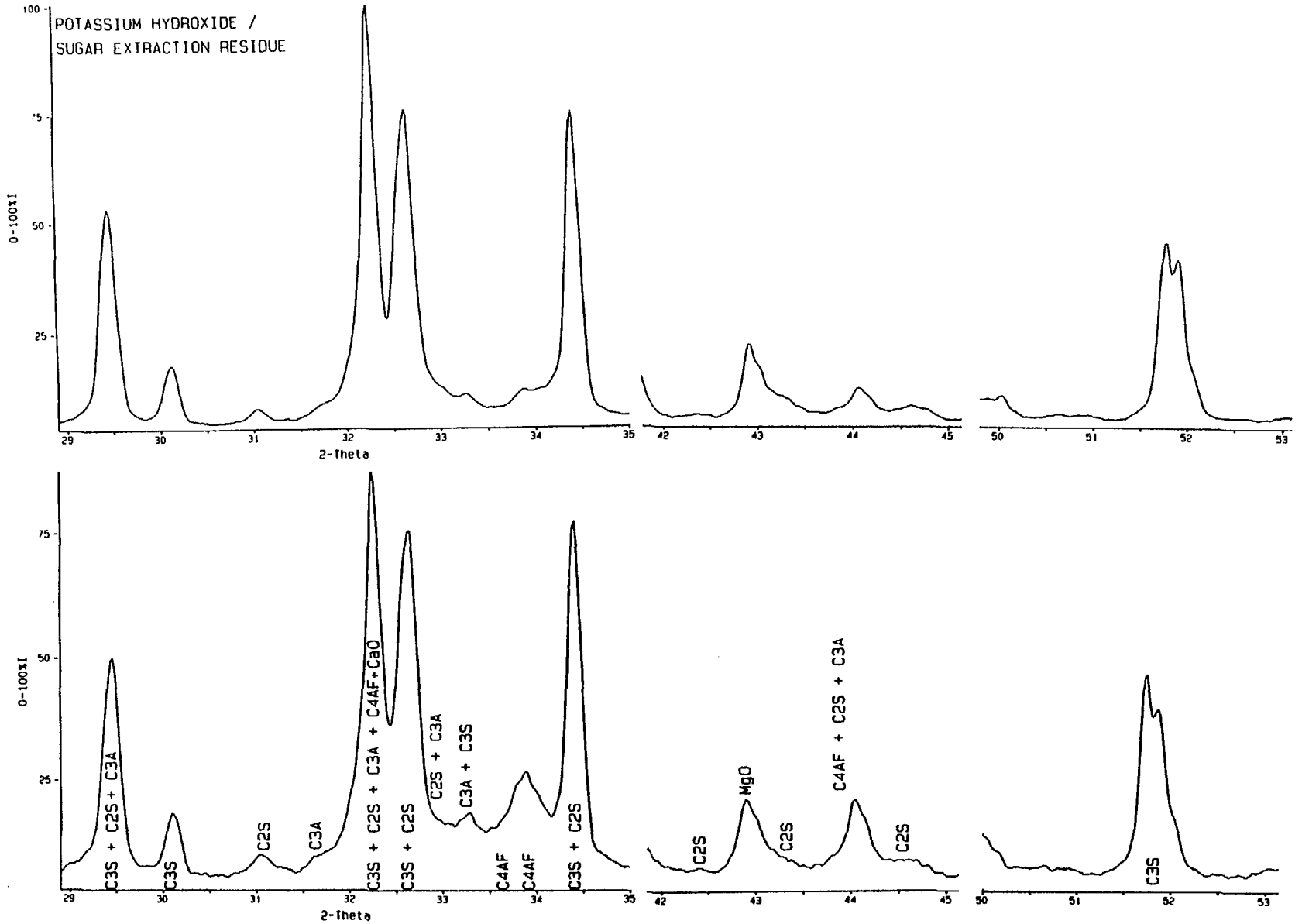

Figure 10. The potassium hydroxide / sugar extraction dissolves the interstitial phases aluminate and ferrite leaving a residue of silicates and periclase.

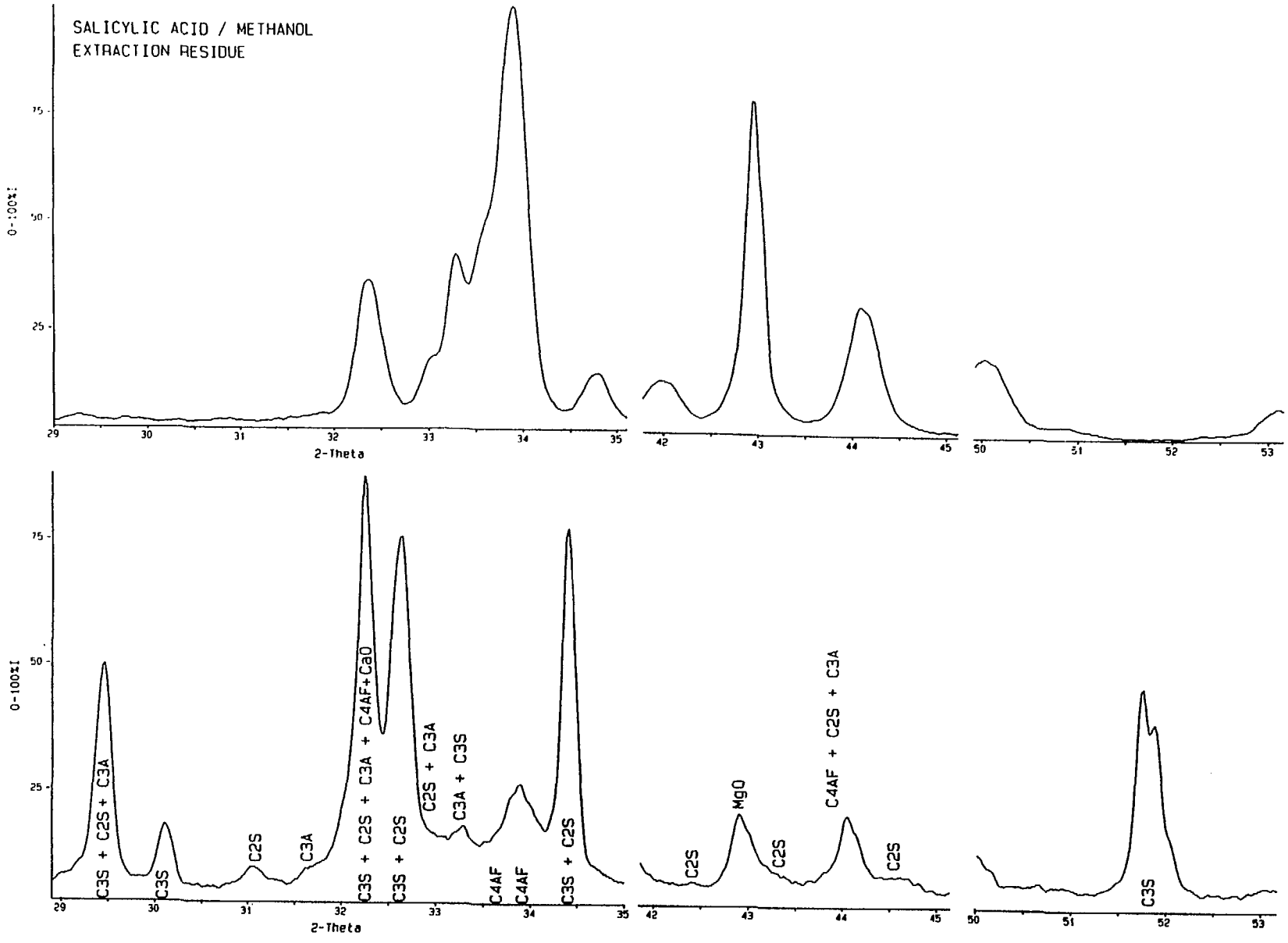

Figure 11. The salicylic acid / methanol extraction dissolves the silicate phases alite and belite, and free lime from the bulk clinker (lower pattern) leaving a residue enriched in ferrite, aluminate, and alkali sulfates.

3.3 Nitric Acid/Methanol Extraction

This extraction dissolves the silicates and aluminates leaving a residue of ferrite and periclase (Fig. 12). Ten grams of ground clinker stirred in 500 ml of 7% nitric acid in methanol for 30 minutes dissolves the silicates and aluminates [11]. An almost pure ferrite residue was obtained from Reference Clinker 8488, and a ferrite and periclase mixture was obtained from RM 8486 using a nitric acid/methanol extraction.

4.0 Evaluating and Monitoring Machine Performance

Control charts provide a means to evaluate and document the X-ray powder diffractometer performance and aid in identification of machine problems such as misalignment and tube deterioration (Fig. 13). A number of certified Standard Reference Materials[5] are available for this purpose and, although not certified, the quartz plate provided by most powder diffractometer manufacturers may also be used to document performance. Certified reference standards are available for evaluation of sensitivity, d-spacing, and quantitative analysis.

Instrument sensitivity is evaluated using SRM 1976, a plate of sintered alumina. Plotting the ratios of measured peak intensities to the certified values as a function of 2θ yields a curve of instrument sensitivity. The trend of the curve indicates if the instrument is "in control" and, if not, may indicate the nature of the problem. Diffractometers with variable incident beam slit systems require correction of the data to fixed slit values before comparison with the certified values. Alternatively, this plate may be used to determine a correction curve to correct variable slit data to fixed slit data.

A method for developing a control chart using SRM 1976 suggested by an ICDD/JCPDS task group [12] may be utilized for quick, routine testing. Our lab procedure is a modification in that it measures three of the diffraction peaks within the typical 2θ range used for cements. An widened 2θ scan range for the (104) peak includes a region where the tungsten X-ray tube contamination peak occurs for the (104) peak. The W $L\alpha_1$ (λ = 0.147639 nm) radiation produces a diffraction peak at 24.49° 2θ. Other values to monitor machine performance include d-spacing accuracy and diffraction peak intensity changes versus time.

---

[5]Standard Reference Materials and Reference Materials specifically for X-ray powder diffraction are available from the National Institute of Standards and Technology (NIST) Standard Reference Materials Program (SRMP), (301) 975-6776.

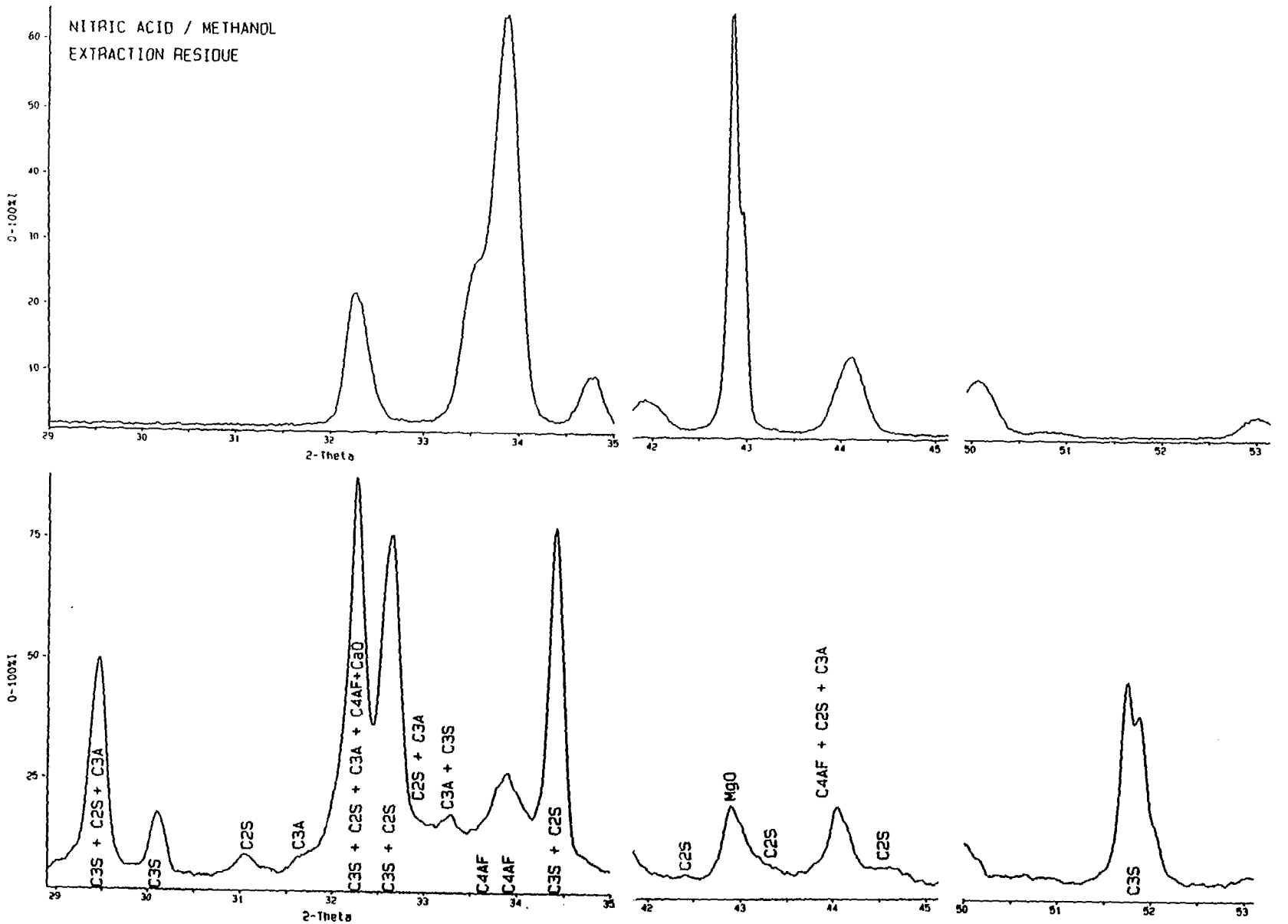

Figure 12. A residue enriched in ferrite and periclase may be obtained using a nitric acid/methanol extraction.

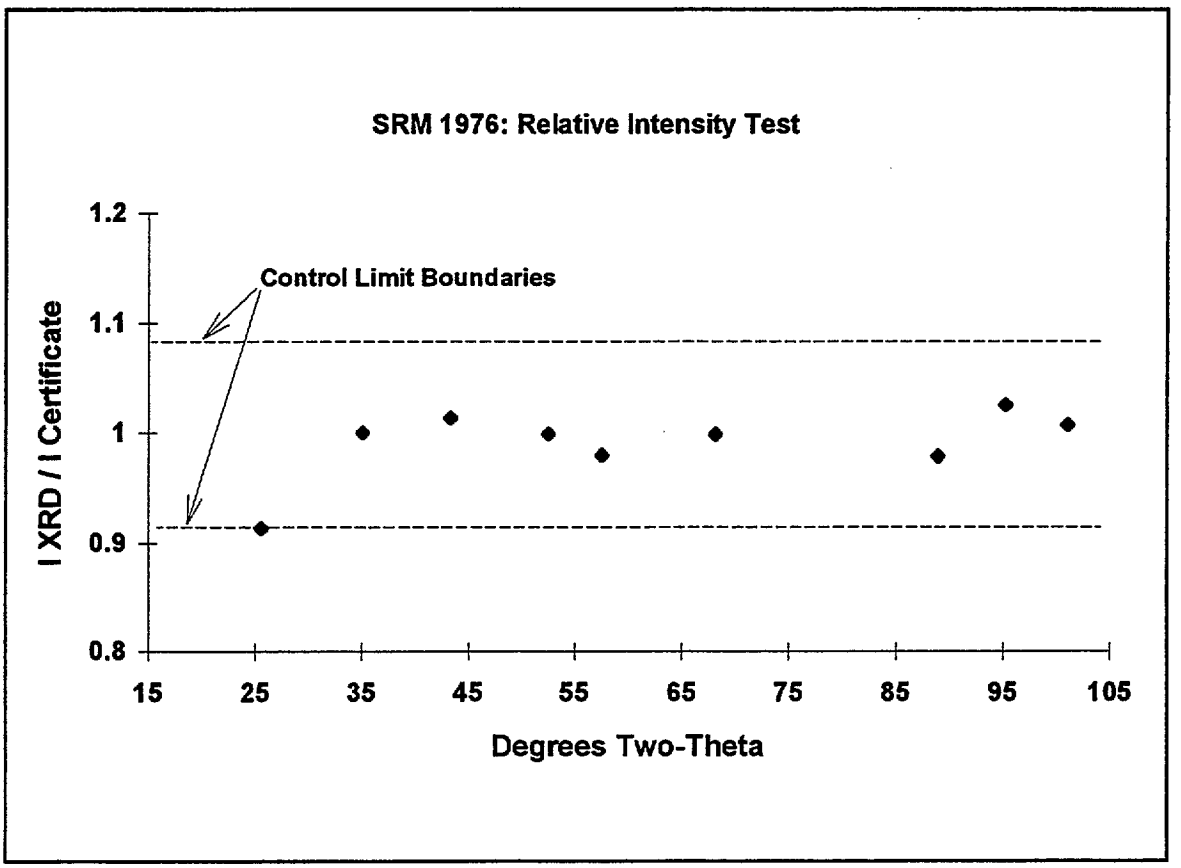

Figure 13. Control Charts for Instrument Sensitivity using SRM 1976 are used to determine machine accuracy in measurement of relative intensities. The lines indicate the upper and lower control limit boundaries as provided in the certificate.

SRMs 640b (silicon) and 675 (mica) are suitable for use as internal or external d-spacing standards. The correction curve is plotted as the difference between measured and certified peak positions as a function of 2θ angle. Large (in excess of a few hundredths of a degree) or anomalous values indicate alignment problems with the diffractometer.

Other SRMs as pure phases suitable for quantitative analysis standards include 1878, α-quartz; 1879, cristobalite; 676, corundum; and 674, a set of powders consisting of corundum (Al_2O_3), wurtzite (ZnO), rutile (TiO_2), and cerium oxide.

5.0 Quantitative Analysis

5.1 The Internal Standard Method for Quantitative Analysis

While peak intensity is proportional to phase concentration, this relationship is usually not linear due to absorption of the X-ray beam by the mixture. The mass absorption coefficient (μ/ρ), a measure of a phase's "stopping power" of an X-ray, is dependent on the composition of the phase. The μ/ρ of a mixture is dependent on the mass fraction of each phase. The latter is difficult to measure, and the mass fraction of the phases are not known. A list of mass absorption coefficients (copper Kα radiation) for cement phases and internal standards are presented in Table 2. In a diffraction pattern with a weak absorber, such as periclase, and a strong absorber, such as rutile, the periclase pattern will appear weaker and the rutile pattern will appear stronger than expected if there were a linear relationship between peak intensity and concentration.

Table 2. Mass Absorption Coefficients, μ/ρ, for Selected Phases Commonly Found in Clinker and Cement, and Internal Standards.

Phase	Composition	μ/ρ
alite	Ca_3SiO_5	92.3
belite	Ca_2SiO_4	89.5
aluminate (cubic)	$Ca_3Al_2O_6$	85.9
aluminate (orthorhombic)	$NaCa_4Al_3O_{10}$	79.0
ferrite (low Al)	$Ca_4Fe_4O_{10}$	177.7
ferrite	$Ca_4FeAl_3O_{10}$	107.1
periclase	MgO	27.8
free lime	CaO	119.1
arcanite	K_2SO_4	84.8
thenardite	Na_2SO_4	35.0
gypsum	$CaSO_4 \cdot 2H_2O$	82.4
bassanite	$2CaSO_4 \cdot H_2O$	70.1
soluble anhydrite	$2CaSO_4 \cdot H_2O$	70.1
anhydrite	$CaSO_4$	74.1
rutile	TiO_2	129.3
corundum	Al_2O_3	31.4
silicon	Si	60.6
fluorite	CaF_2	91.9

Klug and Alexander [4] derived equations for quantitative phase abundance analysis by X-ray powder diffraction showing that the intensity of a diffraction peak i from phase α in a flat, packed powder mixture is given by:

$$I_{i\alpha} = \frac{K_{i\alpha} X_\alpha}{\rho_\alpha \left(\frac{\mu}{\rho}\right) m} \qquad (1)$$

Where,

$I_{i\alpha}$	=	the intensity of diffraction peak i of phase α,
$K_{i\alpha}$	=	a constant dependent on the diffractometer, peak i of phase α, and experimental conditions,
X_α	=	the mass fraction of phase α,
ρ_α	=	the density of phase α, and
$(\mu/\rho)_m$	=	the mass absorption coefficient of the mixture,

Furthermore, they demonstrated that in a multi-component mixture of phases with different μ/ρ values, and where the $(\mu/\rho)_{mixture}$ is unknown, an internal standard (I_s) added to the sample in a known proportion can be used to correct for absorption effects. By taking the peak intensity ratio, $I_{i\alpha}/I_s$, the absorption factors are eliminated. Calibration curves are determined for each phase using mixtures of known phase proportions (x_α and x_s) and fixed proportion of internal standard, and plotting the peak intensity ratio $I_{i\alpha}/I_s$ versus the mass fraction of the phase.

A suitable internal standard for quantitative analysis should be a phase not normally found in the material being analyzed, with few, strong diffraction peaks that do not overlap those in the material. It should not be prone to preferred orientation, and have similar absorption characteristics compared to the unknown material. Compounds commonly used for cement XRD studies include rutile, corundum, silicon, and fluorite.

An ideal calibration mixture set will contain each phase at least three times in mass fractions close to the maximum, minimum, and median values expected in the unknowns. This will provide three points per phase across the range of expected concentrations for definition of the calibration curve.

5.2 The Reference Intensity Ratio Technique

The reference intensity ratio (RIR) technique [13] is an adaptation of the internal standard method. The slope RIR of the calibration plot is given by:

$$\frac{I_{i\alpha}}{I_{js}} \frac{I_{js}^{rel}}{I_{i\alpha}^{rel}} \frac{X_s}{X_\alpha} = RIR_{\alpha,s} \qquad (2)$$

where:

I^{rel}_{js} = relative peak intensity of diffraction peak j of internal standard s,
$I^{rel}_{i\alpha}$ = peak intensity of diffraction peak i of phase α,
X_α = mass fraction of phase α, and
X_s = mass fraction of internal standard s,

According to the traditional ICDD definition, the RIR value reflects the intensity ratio of the strongest peak of a phase to that of corundum. However, resolving the most intense peak for any phase in a cement pattern is difficult at best, and corundum might not be selected as an internal standard. For cement analyses, the RIR may then be defined as the intensity ratio of the strongest resolvable diffraction peak to that of an internal standard. Knowledge of relative peak intensities, best determined experimentally, allows calculation of a single phase intensity based on the most intense peak and therefore a single RIR value for each phase. In cases where only one peak is used, the relative intensity correction is not necessary.

Calibration using the RIR method requires three steps:

a) collection of diffraction patterns of individual phases for measurement of background-subtracted relative intensities;
b) collection of diffraction patterns of multi-phase mixtures of known composition intermixed with a known mass of internal standard; and
c) calculation of peak or pattern intensities and calculation of the RIR constant relating peak intensity ratio with mass fraction ratio using eq. (2).

Analysis of the unknown mixture involves the following:

a) addition and homogenization of a known mass of internal standard;
b) three replicate diffraction scans, repacking for each;
c) measurement of background-subtracted intensities; and
d) calculation of the mass fraction of each phase using eq. (3):

$$\frac{I_{i\alpha}}{I_{js}} \frac{I_{js}^{rel}}{I_{i\alpha}^{rel}} \frac{X_s}{RIR_{\alpha,s}} = X_\alpha \qquad (3)$$

An advantage of the RIR technique is flexibility in addition of the internal standard. While the mass fraction of internal standard needs to be known, it need not be fixed. X_s in eq. 3 is the mass fraction of internal standard in the composite mixture, so a 10 percent addition internal standard to an unknown comprises 9.09 percent of the mixture. Mass fractions of the unknown are of a mixture <u>including</u> the internal standard. Correct for the internal standard using eq. (4):

$$\frac{X_\alpha}{(1-X_s)} = X_\alpha' \quad (4)$$

6.0 Data Collection

The 2θ scan range is selected to encompass the strong diffraction peaks and regions representative of the pattern background. Measurement of intensities requires careful placement of the background curve, separation of overlapping diffraction peaks, subtraction of the background under each peak, measurement of the peak area. As X-ray generation is a random process, the net error in counting is an inverse function of the total counts measured at each step or for each peak area. The random error is proportional to $N^{-1/2}$ where N is the total count after background subtraction [4]. Therefore, the greater the number of counts at each step, the greater the precision of the measurement.

6.1 Pattern Intensity Measurement

6.1.1 Peak Area Measurement

Methods for intensity measurement include peak height or peak area measurement using a planimeter or profile fitting. Peak area measurement is generally accepted as the best measurement technique because it is least influenced by particle size. First, the background needs to be fit to the pattern. This is accomplished by fitting a smooth curve to regions of true background. The overlapping of peaks does not always allow the diffraction intensity to return to a true background between peaks, so selection of a scan range that includes background regions aids in this operation. Next, overlapping peaks need to be resolved by manual interpolation to the background or through profile fitting, and the background-subtracted peak area measured (Fig. 14). Difficulty in the ability of manual interpolation and in profile-fitting algorithms to resolve severely overlapped peaks limits these methods to the less intense diffraction peaks.

6.1.2 Whole-Pattern Fitting

An alternative technique involves the fitting of entire diffraction patterns on a point-by-point basis. A linear least-squares fit of a set of pure phase diffraction patterns to that of the clinker or cement mixture provides weights of each pattern comprising the mixture. The quality of fit is calculated as a residual error value and displayed as a difference plot. Figure 15 illustrates this application in measurement of pattern intensities for cubic and orthorhombic aluminates. The differences between reference and cement phase diffraction patterns reflect compositional and structural variations but, use of the entire pattern should lessen the influence of any single peak in estimation of the pattern intensity. For individual peak measurement, the peaks noted as resolvable are also thought to be less sensitive to these variations [14]. Gutteridge [15] used a set of reference phases determining the best combination of references by selecting the reference set producing the lowest residual error.

6.2 Rietveld Method

The Rietveld method uses the entire diffraction pattern but differs in that it also calculates best-fit diffraction patterns by refining models for crystal structure, instrument influences, and specimen characteristics [16,17,18]. Some knowledge of the crystal structure of each phase is necessary, and information on the refined crystal structure, unit cell parameters, and approximate chemical compositions for each phase are determined. Taylor and Aldridge [17] have applied Rietveld analysis in the investigation of alite polymorphs in cement.

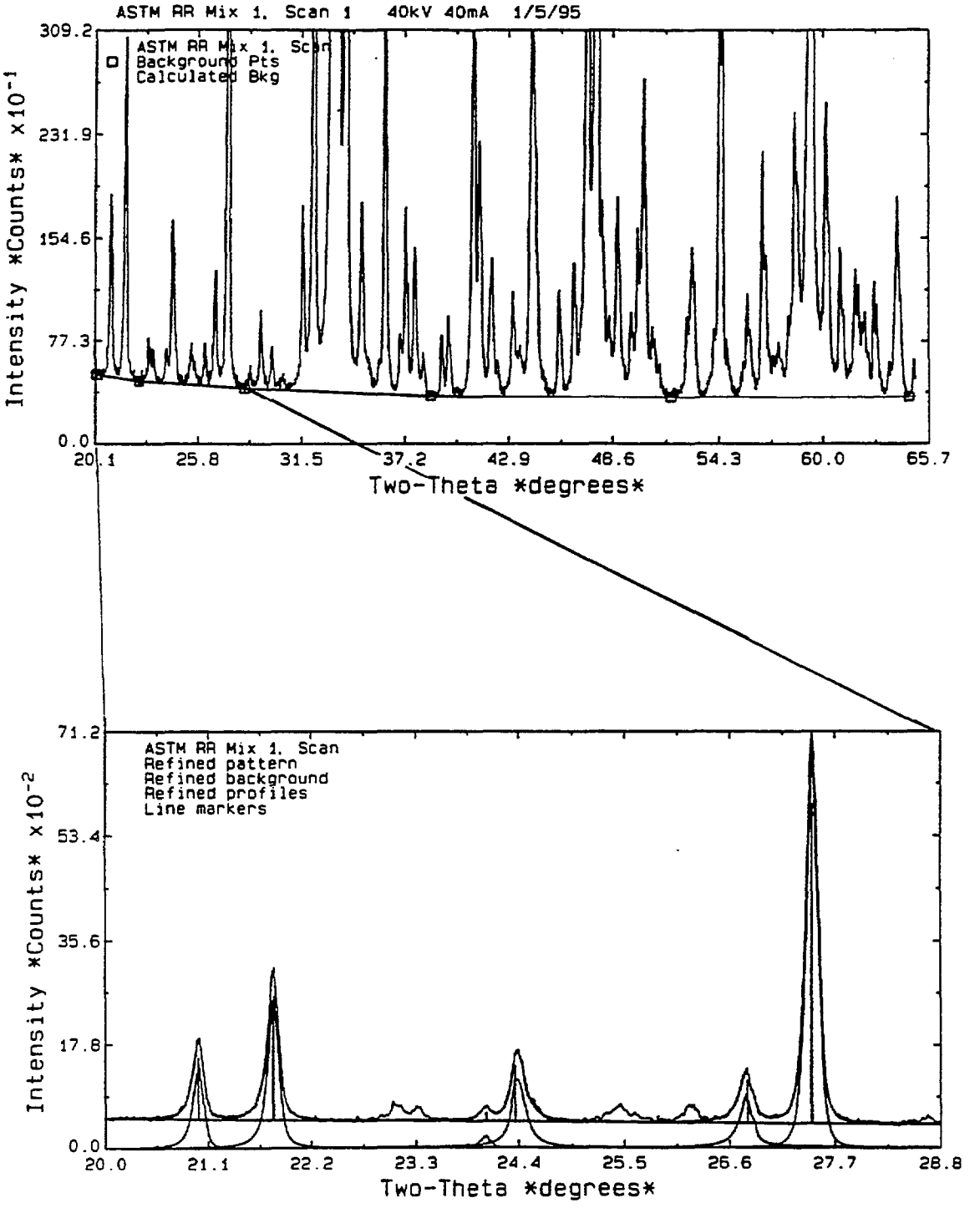

Figure 14. Background is fitted as a smooth curve to points selected as representative of the actual background. Peaks are resolved and background-subtracted peak areas calculated.

7.0 ASTM C01.23.01 Cooperative Calibration

The cooperative calibration dataset from the Building and Fire Research Laboratory is presented here to illustrate procedures for calibration and analysis of the unknown mixtures. The cooperative calibration was initiated by the ASTM C01.23.01 task group on X-ray powder diffraction as part of an effort to develop a test method for quantitative analysis of clinker and cement phase abundance. The calibration and analysis of unknowns will be used to establish precision and accuracy levels of the test method. The first part involves calibration for interstitial phases of cubic and orthorhombic aluminate, ferrite, and MgO. Participants will then proceed to analyze SAX residues from the NIST Reference Clinkers. Later, the task group will add the silicates, then calcium sulfates and alkali sulfates.

Five mixtures were prepared by Construction Technology Laboratories, three of known phase composition for calibration, two mixtures as unknowns. Participants were instructed to follow a procedure requiring an internal standard (IS) addition. The choice of IS, the mass fraction IS addition, scan conditions, and peaks for intensity measurement were selected by each laboratory. Our selection of rutile as an IS was based on the use of three resolvable diffraction peaks (27.45°, 36.09°, and 54.32° 2θ), its similar mass absorption coefficient to phases found in portland cement, and material availability.

Calibration mixtures were intermixed with a 12% IS addition, proportioned using a 5-place analytical balance, and homogenized by mortar and pestle using a 200 proof ethanol slurry. Each calibration mixture was then placed in a glass vial labeled with sample name, the IS type and mass fraction addition, and date of preparation. The vials were capped loosely and stored in a vacuum desiccator. Mixtures of the two unknowns were prepared in a similar manner.

Three replicate powder mounts were prepared for each mixture and diffraction scans collected using a Philips diffractometer at 40kV and 40mA, 0.02° step, and a 5-second count time. Background profiles were fitted using a spline function interpolating between points selected as background. Intensity measurements are made using the least-squares pattern fitting of a set of pure phase reference patterns.

When measuring individual peak intensities the quantitative determination of aluminate polymorphs may follow a procedure recommended by the task group (Fig. 15). Orthorhombic aluminate produces a peak at 21.0° that overlaps that from cubic aluminate. Measurement of the cubic aluminate intensity ratio (I 21.0°/I 21.8°) is made from calibration mixture 1, which contains only cubic aluminate. The peak intensity (I 21.0°) exceeding the cubic aluminate ratio is attributed to orthorhombic aluminate. Other peaks for orthorhombic aluminate that may aid in identification include those at 20.15° and 17.35° 2θ.

The calibration data (Table 3) are then plotted as the pattern intensity ratio versus mass fraction ratio. When the mass fraction of internal standard is held constant, the calibration plot may presented as peak intensity ratio versus mass fraction of the unknown phase (Fig. 16). A least-squares fit of a line to the data points provides the calibration relating intensity ratio to mass fraction of the unknown phase. The alternative means of representing this relationship through the single RIR value is discussed in section 5.2.

Table 4 presents results of the analysis of the two unknowns. The ability of these calibrations to predict the mass fractions of the phases of the two unknown mixtures is good with absolute errors, based on the whole cement, below 1 percent. Some bias is present as some of the calculated mass fractions fall outside the standard deviation reproducability range. The identification of orthorhombic aluminate in unknown sample 1 was made by a number of participants in the round robin and illustrates a need to examine lower detection limits. Additional calibration points in this mass fraction range should improve these results.

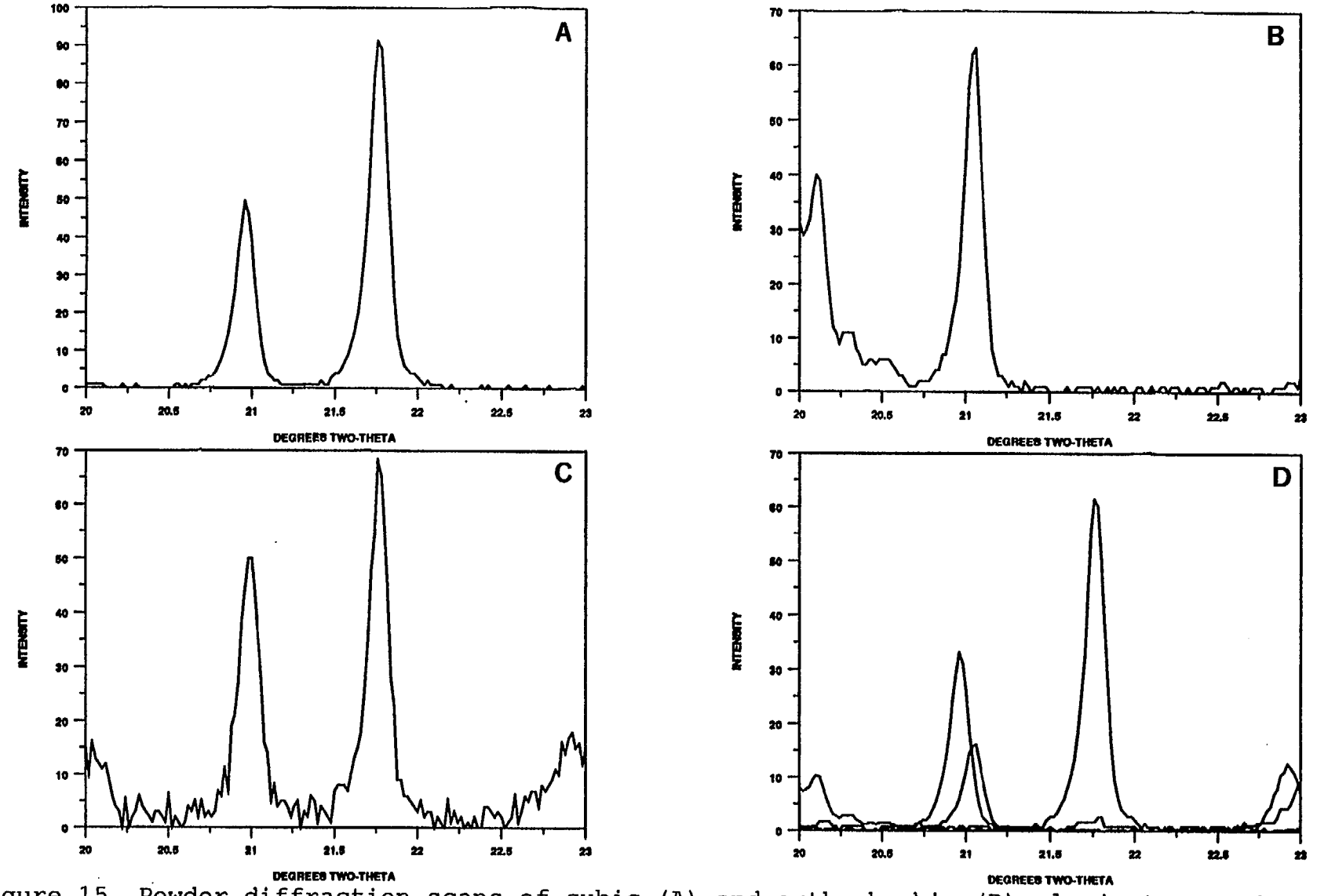

Figure 15. Powder diffraction scans of cubic (A) and orthorhombic (B) aluminates, and a mixture containing both polymorphs (C). As the I 21.0°/I 21.8° ratio exceeds that of pure cubic aluminate (about 0.5), orthorhombic aluminate may be considered to be present (D).

Table 3. Dataset for the Cooperative Calibration

Known Mixture 1

Phase	Mass	Pattern Intensity Scan 1	Scan 2	Scan 3	Intensity Ratios I/I TiO_2 1	I/I TiO_2 2	I/I TiO_2 3	Average I/I TiO_2	Std. Dev.
C_3A-Cubic	65	0.985860	0.984324	0.980169	4.722502	4.736061	4.705474	4.721346	0.0153
C_4AF	35	0.354054	0.351141	0.357382	1.696002	1.689510	1.715675	1.700396	0.0136
Rutile (IS)	12	0.208758	0.207836	0.208304					
C_3A-Cubic 21.8°/20.9° intensity ratio					0.50056	0.52103	0.49746	0.50635	

Known Mixture 2

Phase	Mass	Pattern Intensity Scan 1	Scan 2	Scan 3	Intensity Ratios I/I TiO_2 1	I/I TiO_2 2	I/I TiO_2 3	Average I/I TiO_2	Std. Dev.
C_3A-Cubic	11	0.340935	0.350029	0.350460	0.861711	0.874611	0.869703	0.868675	0.0065
C_3A-Ort.	51	0.700826	0.696038	0.699160	1.771333	1.739178	1.735039	1.748516	0.0199
C_4AF	11	0.217044	0.219552	0.216170	0.548577	0.548591	0.536449	0.544539	0.0070
MgO	27	0.644960	0.641183	0.64323	1.630132	1.602112	1.596243	1.609496	0.0181
Rutile (IS)	12	0.395649	0.400211	0.402965					

Known Mixture 3

Phase	Mass	Pattern Intensity Scan 1	Scan 2	Scan 3	Intensity Ratios I/I TiO_2 1	I/I TiO_2 2	I/I TiO_2 3	Average I/I TiO_2	Std. Dev.
C_3A-Cubic	29	0.692944	0.680578	0.690178	1.919034	1.905826	1.917012	1.913957	0.0071
C_3A-Ort.	7	0.145421	0.138934	0.133077	0.402728	0.389058	0.369630	0.387138	0.0166
C_4AF	60	1.011120	0.998785	1.003280	2.800188	2.796902	2.786672	2.794588	0.0070
MgO	4	0.087225	0.084298	0.083400	0.241560	0.236060	0.231648	0.236423	0.0050
Rutile (IS)	12	0.361090	0.357104	0.360028					

Summary

Mass	C_3A-Cubic I/I TiO_2	RIR	Mass	C_3A-Ort. I/I TiO_2	RIR	Mass	C_4AF I/I TiO_2	RIR	Mass	MgO I/I TiO_2	RIR
11	0.868675	0.947650	7	0.387138	0.663667	11	0.544539	0.594045	4	0.236423	0.709274
29	1.913957	0.791982	51	1.748516	0.411416	35	1.700396	0.582994	27	1.609496	0.715334
65	4.721346	0.871634				60	2.794588	0.558919			

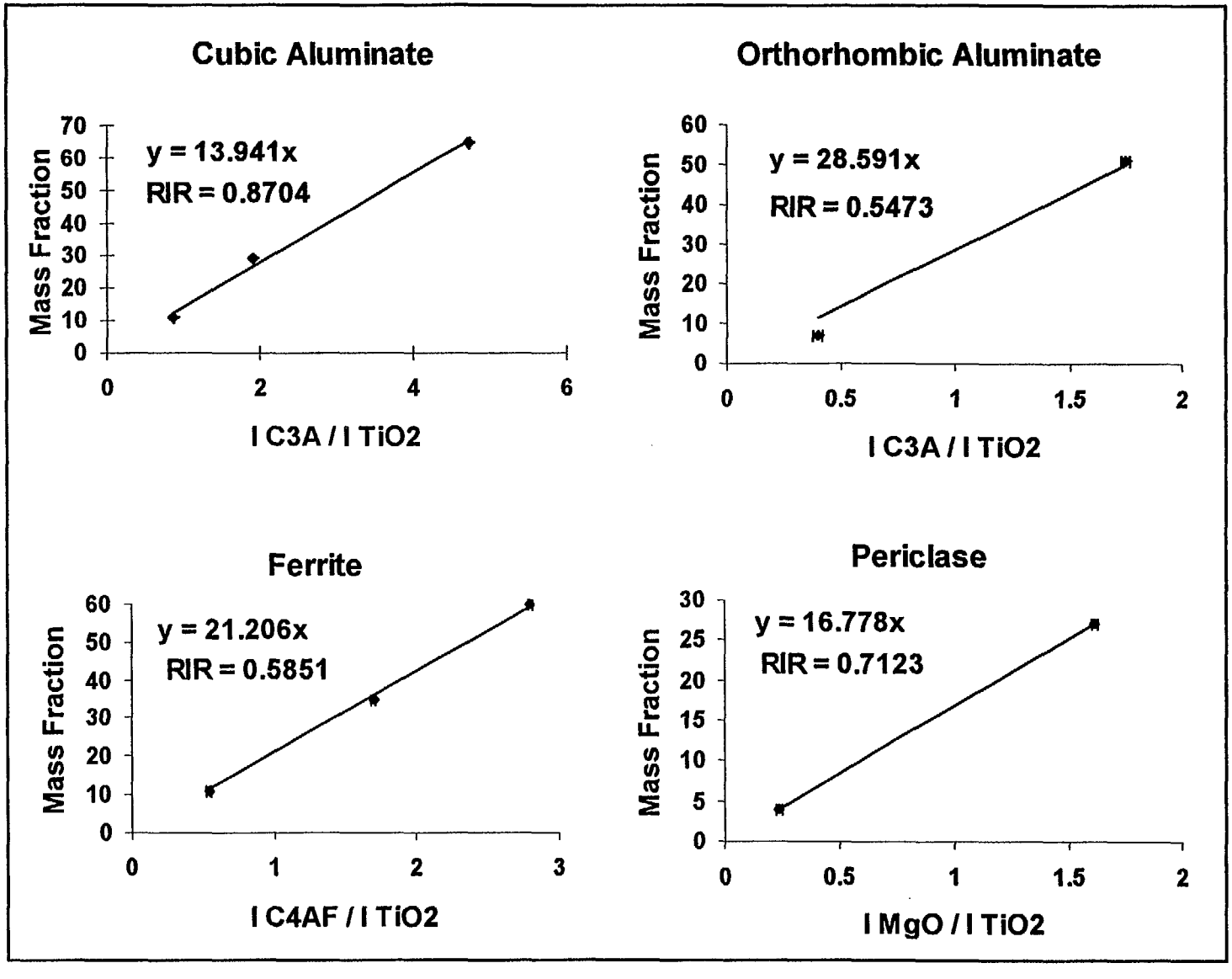

Figure 16. Calibration Curves and RIR Values for ASTM Round Robin Calibration

Table 4. X-Ray Powder Diffraction Intensity Data for Unknowns

Unknown Mixture 1

	Mass Fraction*			Bulk Cement**			Intensity		
	Calc.	St.Dev.	Known	Calc.	Known	Abs. Error	1	2	3
C_3A-Cubic	18.7	0.1	20.0	3.2	3.4	0.2	0.490770	0.507575	0.491604
C_3A-Ort.	3.1	0.8	0.0	0.5	0.0	0.5	0.036517	0.066263	0.053034
C_4AF	57.8	1.6	58.0	9.8	9.9	0.1	0.984071	1.085670	1.008950
MgO	21.3	0.6	22.0	3.6	3.7	0.1	0.449247	0.490535	0.460795
Rutile							0.366017	0.383479	0.370975

Unknown Mixture 2

	Mass Fraction			Bulk Cement			Intensity		
	Calc.	St.Dev.	Known	Calc.	Known	Abs. Error	1	2	3
C_3A-Cubic	63.8	1.5	63.0	10.8	10.7	0.1	0.903482	0.886955	0.903967
C_3A-Ort.	8.6	0.6	7.0	1.5	1.2	0.3	0.068008	0.071737	0.081774
C_4AF	26.7	0.6	26.0	4.5	4.4	0.1	0.247737	0.243913	0.254705
MgO	4.2	0.1	4.0	0.7	0.7	0.1	0.047324	0.048724	0.049207
Rutile							0.199042	0.191529	0.193963

* values rounded to the nearest tenth

** Bulk cement values are recalculated mass fractions to that of the bulk cement, that is, the unextracted cement specimen.

8.0 Summary and Conclusions

Correlation of cement composition with performance characteristics necessitates the development of accurate methods of phase abundance analysis. X-ray powder diffraction is a direct method, and for fine-grained materials it is the only method for direct qualitative and quantitative phase composition analysis. While the application of XRD in the cement industry in qualitative analysis is well established, its use in quantitative analysis is not common. This guide provides an outline for the quantitative analysis of clinker and cement ranging from sample preparation to phase identification to quantitative analysis.

Calibration and measurement of compositions are illustrated using the ASTM QXRD task group cooperative calibration sample set. This set represents an ideal model for QXRD analysis, as the calibration samples are comprised of the same compounds in the unknowns. The ability of these calibrations to predict the mass fractions of the phases of the two unknown mixtures is good with absolute errors, based on the whole cement, below 1 percent.

The increase in standard deviation of intensity ratios from replicate scans of the same specimen without repacking to that where the powder was repacked indicates a sample-related variation. This may reflect the limited sampling volume due to absorption and resulting sample heterogeneity. Improved grinding methods that will produce finer particle sizes without damage will help in reducing this problem.

Compositional and structural variations found in industrial clinkers may result in lower accuracy unless comparable phases for reference standards can be secured. This is not unreasonable, as selective extractions allow concentration of individual phases or groups of phases. Given proper reference standards, quantitative phase abundance measurements by X-ray powder diffraction are possible.

9.0 Acknowledgements

Support for this work was provided by NIST and the High Performance Construction Materials and Systems Program. I would also like to thank reviewers Mary McKnight, Ken Snyder of NIST and Fulvio Tang of Construction Technology Laboratories for their comments and suggestions on improvements in this paper.

10.0 References

1. Taylor, H.F.W., Cement Chemistry, Academic Press Limited, London, 1990.

2. Struble, L.J., "Quantitative Phase Analysis of Clinker Using X-Ray Diffraction," Cement, Concrete, and Aggregates. Vol. 13, No. 2, Winter, 1991, pp. 97-102.

3. Struble, L.J., "Cooperative Calibration and Analysis of Cement Clinker Phases, Report 2," Civil Engineering Studies Structural Research Series No. 556, University of Illinois, Sept. 1990, 21 pp.

4. Klug, H.P., and Alexander, L.E., X-Ray Diffraction Procedures, John Wiley and Sons, New York, 1974.

5. Bish, D.L. and Reynolds, R.C. Jr., "Sample Preparation for X-Ray Diffraction," in Reviews in Mineralogy, D.L. Bish and J.E. Post, eds., Vol. 20, pp. 73-99, 1989.

6. "Guide to Compounds of Interest in Cement and Concrete Research," Special Report 127, Highway Research Board, Washington, D.C., 1972, 53 pp.

7. International Center for Diffraction Data/Joint Committee for Powder Diffraction Standards (ICDD/JCPDS), Newton Square, PA.

8. DeHayes, S.M., "Hydraulic Cement - Chemical Properites," in P. Klieger and J.F. Lamond, eds., Significance of Tests and Properties of Concrete and Concrete-Making Materials, ASTM STP 169C, American Society for Testing and Materials, 1994.

9. Deer, W.A., Howie, R.A., and J. Zussman, An Introduction to the Rock-Forming Minerals, Longman Group Limited, Essex, 1985, 528 pp.

10. Gutteridge, W.A., "On the Dissolution of the Interstitial Phases in Portland Cement," Cement and Concrete Research, Vol. 9, pp. 319-324, 1979.

11. Klemm, W.A. and J. Skalney, "Selective Dissolution of Clinker Minerals and Its Applications," Martin Marietta Technical Report 77-32, 30 pp., 1977.

12. Blanton, T.N., W.N. Schreiner, J.N. Dann, G.P. Hamill, and R.F. Hamilton, "JCPDS - International Center for Diffraction Data Statistical Process Control Method Development" Powder Diffraction 8 (4), December, 1993, pp. 229-235.

13. Snyder, R.L. and D.L. Bish, "Quantitative Analysis" in Reviews in Mineralogy, D.L. Bish and J.E. Post eds., Vol. 20, pp. 101-144, 1989.

14. Struble, L.J., Personal communication

15. Gutteridge, W.A., "Quantitative X-Ray Powder Diffraction in the Study of some Cementitive Materials," British Ceramics Proceedings [35], 11-23, 1984.

16. Post, J.E. and D.L. Bish, "Rietveld Refinement of Crystal Structures Using X-Ray Diffraction Data," in Reviews in Mineralogy, D.L. Bish and J.E. Post eds., Vol. 20, pp. 277-305, 1989.

17. Taylor, J.C. and L.P. Aldridge, "Full Profile Rietveld Quantitative XRD Analysis of Portland Cement: Standard XRD Profiles for the Major Phase Tricalcium Silicate (C_3S: $3CaO.SiO_2$)," Powder Diffraction 8 (3) 1993, pp. 138-144.

18. Young, R.A., "Introduction to the Rietveld Method," in The Rietveld Method, R.A. Young, Ed., IUCr Monographs on Crystallography No. 5., Oxford University Press, 1993, pp. 1-38.